universität wien

DIPLOMARBEIT

Titel der Diplomarbeit

„Preclinical evaluation of [^{18}F]FE@SUPPY and [^{18}F]FE@SUPPY:2 with Autoradiography“

verfasst von

Elisabeth Szerencsics

angestrebter akademischer Grad

Magistra der Pharmazie (Mag.pharm.)

Wien, März 2014

Studienkennzahl lt. Studienblatt:	A 000449
Studienrichtung lt. Studienblatt:	Pharmazie
Betreut von:	o.Univ.-Prof. Mag.pharm. Dr. Helmut Viernstein

Danksagung

An dieser Stelle möchte ich mich bei all den wunderbaren Menschen bedanken, die an der Entstehung dieser Diplomarbeit beteiligt waren.

Ein recht herzliches Dankeschön gilt O.Univ. Prof. Mag.pharm. Dr. Helmut Viernstein, der mir eine Stelle als Diplomandin am Department of Pharmaceutical Technology and Biopharmaceutics zur Verfügung gestellt hat.

Bei Univ. Doz. Mag.pharm. Dr. Markus Mitterhauser möchte ich mich hiermit für umfassende Unterstützung, die guten Ratschläge, die aufmunternden Worte und die schöne Zeit in der Arbeitsgruppe der Radiopharmaceutical Sciences bedanken.

Ein Dankeschön gebührt Mag. Dr. Wolfgang Wadsak für die zahlreichen Hilfestellungen und den Beistand während der stundenlangen Auswertungen.

Ein besonderer Dank geht an Mag. pharm. Dr. Daniela Häusler für die fachliche und persönliche Betreuung und für ihr Engagement den Bereich der Autoradiographie in der Arbeitsgruppe zu etablieren.

Mag. Dr. Johanna Ungersböck hat durch ihre Fürsorge und ihre Persönlichkeit meine Zeit in der Arbeitsgruppe mit schönen und unvergesslichen Erinnerungen gefüllt, wofür ich ihr hiermit meinen Dank aussprechen möchte. Weiters möchte ich mich auch bei Friedrich Girschele bedanken, welcher mir immer mit Rat und Tat zur Seite gestanden ist.

Ein großes Dankeschön gilt der gesamten Arbeitsgruppe für die mentale Unterstützung und für das angenehme Arbeitsumfeld.

Am Ende möchte ich mich noch bei all meinen Freunden und natürlich bei meiner Familie bedanken. Ein Dankeschön gilt meiner Schwester Margit, welche mir den letzten Tritt zum Studienende verpasst hat, meinen Brüdern Horst und Rainer, die mir immer Rückendeckung gegeben haben und natürlich meinen Eltern, ohne deren Hilfe dieses Studium nicht möglich gewesen wäre und die mir durch ihren unerschütterlichen Glauben an mich und meine Fähigkeiten den notwendigen Rückhalt gegeben haben.

Zusammenfassung

Adenosinrezeptoren spielen eine vielseitige Rolle im menschlichen Organismus. Agonisten und Antagonisten an diesen Rezeptoren stellen mögliche Therapeutika für unterschiedliche Erkrankungen dar. Die vielseitigen Funktionen des Adenosin A_3 Rezeptors (A_3AR) umfassen unter anderem eine zellschützende, entzündungshemmende, antikanzerogene und kardioprotektive Wirkung. [^{18}F]FE@SUPPY wurde als erster PET-Tracer für den A_3AR synthetisiert. [^{18}F]FE@SUPPY:2 ist eine Variante des [^{18}F]FE@SUPPY, welche statt an der Carbonsäureestergruppe an der Thioester-Funktion eine radioaktive Markierung trägt. Es wurde bei diesem Isomer erwartet, dass es ein gleiches Bindungspotenzial und gleiche pharmakologischen Eigenschaften wie [^{18}F]FE@SUPPY aufweisen würde. Im Rahmen dieser Diplomarbeit wurden Autoradiographien mit [^{18}F]FE@SUPPY und [^{18}F]FE@SUPPY:2 und [^{125}I]-AB-MECA an Organschnitten von Rattenhirn, Rattenhoden und Rattenherz durchgeführt. Um Vergleiche ziehen zu können, wurden die Versuche durch Zugabe der Antagonisten FE@SUPPY, FE@SUPPY:2, MRS1191 und des Agonisten I-AB-MECA durchgeführt. Zusätzlich wurden Antagonisten der Adenosinrezeptoren A_1, A_{2A} und A_{2B} hinzugefügt um eine selektive Bindung am A_3AR zu gewährleisten. Bei Experimenten mit [^{18}F]FE@SUPPY und [^{18}F]FE@SUPPY:2 zeigten die beiden Radiotracer einen hohen Grad an unspezifischer Bindung, was zu Resultaten mit wenig Aussagekraft führte. Tendenziell zeigten die Experimente mit [^{18}F]FE@SUPPY am Rattenhirn eine bessere Fähigkeit des FE@SUPPY:2 den A_3AR zu blockieren als MRS 1191. Auch die Experimente mit [^{18}F]FE@SUPPY:2 zeigten den Trend, dass FE@SUPPY besser als Antagonist agiert als MRS 1191. Die Experimente am Rattenherz, Rattenhoden und Rattenhirn mit [^{125}I]-AB-MECA wiesen auf eine bessere Fähigkeit des FE@SUPPY hin, den Agonisten vom A_3AR zu verdrängen als MRS 1191, während sich FE@SUPPY:2 als weniger effizienter Antagonist des A_3AR zeigte, als MRS 1191. Diese Resultate heben hervor, dass sowohl [^{18}F]FE@SUPPY, als auch [^{18}F]FE@SUPPY:2 gute Qualitäten als Antagonisten vorweisen, sich die weitere Forschung jedoch auf weniger lipophile Derivate beschränken sollte.

Abstract

Adenosine receptors (ARs) play a versatile role in the human body. Antagonists and agonists represent a promising target for pharmacological intervention in several pathophysiological conditions. Functions of ARs comprise cytoprotective, anti-inflammatory, anticancerogene and cardioprotective effects. [^{18}F]FE@SUPPY was the first PET-Tracer targeting the Adenosine A_3 Receptor. [^{18}F]FE@SUPPY:2 is the isomer of [^{18}F]FE@SUPPY, with the thioester-moiety radioactively labeled instead of the carboxylic function. Regardless of this difference in the structure, the compound was expected to show similar affinity for the A_3AR and similar pharmacological properties. Within this thesis, experiments with [^{18}F]FE@SUPPY und [^{18}F]FE@SUPPY:2 and [^{125}I]-AB-MECA have been performed on slices of rat heart, rat testis and rat brain by autoradiography. The blocking agents FE@SUPPY, FE@SUPPY:2 and MRS1191 have been added as well as the agonist I-AB-MECA, to compare the ability of the radiotracers to block A_3AR. Blocking agents were used to block the Adenosine Receptors A_1, A_{2A} and A_{2B} to display selective imaging of the A_3AR. Experiments with [^{18}F]FE@SUPPY and [^{18}F]FE@SUPPY:2 showed high unspecific binding resulting in insignificant results. Studies with [^{18}F]FE@SUPPY on rat brain slices showed higher competency in blocking A_3AR with FE@SUPPY:2 than with MRS 1191.Experiments with [^{18}F]FE@SUPPY:2 on rat brain slices showed a tendency to better block A_3AR than MRS 1191. Experiments on rat heart, rat testis and rat brain with [^{125}I]-AB-MECA showed better abilities of FE@SUPPY as antagonist than MRS 1191 while FE@SUPPY:2 turned out to be less effective in blocking A_3AR. Results proved the capability of FE@SUPPY and FE@SUPPY:2 to block A_3AR but suggest to focus on less lipophilic derivatives.

Content

1. Introduction

1.1. Adenosine, Receptors and Ligands

Adenosine is a well-researched cytoprotective regulator and acts under both physiological and pathophysiological conditions. The protective response results as a reaction to stress on an organ or tissue. [1] Some of the adenosine induced answers comprise increased ratio of oxygen supply to demand, cell conditioning to protect against ischaemic damage, suppression of inflammation. [1, 2]

The endogenous nucleoside Adenosine, described as 6-Amino-9-β-D-ribofuranosyl-9-H-purine, is composed of an adenine which is bound by a beta-glycosidic binding to a ribofuranyl moiety. [3, 4]

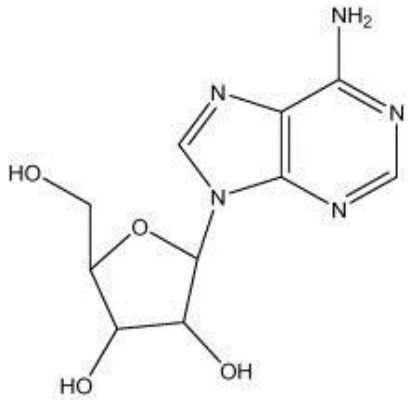

Figure 1 6-Amino-9-β-D-ribofuranosyl-9-H-purine [4]

Adenosine is binding to four subtypes of the Adenosine Receptors (ARs) which are members of the superfamily of G-protein-coupled-receptors (GPCR) coupled to intracellular signalling pathways. [1] The four subtypes of the Adenosine Receptors (ARs) are classified by now as Adenosine A_1-, A_{2A}-, A_{2B}-and A_3-Receptor. [5] The Adenosine Receptors A_1AR and A_2AR were first identified in the 1970s by Van Calker et al. and differentiated among other criteria by structure-activity relationship. [6, 7]

The subclassification of the A_2-Adenosine Receptor (A_2AR) was implemented in the 1980s after discovering activation by high and low concentration of adenosine and adenosine-analogues. [7] The A_3-Receptor subtype was discovered in the 1990s after identifying rat cDNA sequences via polymerase-chain reaction (PCR). These sequences turned out to encode for a guanine nucleotide-binding regulatory protein-coupled

receptor. Further research demonstrated high sequence identity (58%) with the previously identified adenosine receptors but different pharmacological properties. [5]

The ARs, like every GPCR, have a single polypeptide chain forming seven transmembran helices with an extracellular N-terminus and a cytosolic C-terminus. The helices consist of 25-30 amino acids and are connected by three intracellular and three extracellular loops. Within the extracellular region posttranslational modification such as glycosylation are accomplished. The C-terminal domains of A_1- and A_3- ARs hold sites for palmitoylation. [1]

The sequence of the human A_1AR and A_3ARs are up to 49% identical and the human A_{2A}AR and A_{2B}AR are 59% identical. [2] The homology sequences of the A_3AR appear to be only 74% identical between rat and human or sheep and show a 85% homology between sheep and human. The peripheral distribution differs between species e.g. the rat transcript has been identified in testis, lung, kidneys, heart, brain and circulating inflammatory cells. [5] Distribution of A_3ARs in rat tissue is much higher in testis than in lung, kidney and heart. Little distribution of A_3 ARs can be found in rat brain. High distribution of human A_3ARs can be found in lung, liver and placenta. Smaller amounts are located in brain, aorta and kidney. In human testis only little distribution of A_3ARs can be detected and less in human heart. [8]

Expression level	A_1 receptors	A_{2A} receptors	A_{2B} receptors	A_3 receptors
High expression	Brain (cortex, hippocampus, cerebellum), spinal cord, eye, adrenal gland, atria	Blood platelets, olfactory bulb, spleen, thymus, leucocytes	Cecum, colon, bladder	Testis (rat), mastcells (rat)
Intermediate expression	Other brain regions, skeletal muscles, liver, kidney, adipose tissue	Heart, lung, blood vessels, peripheral nerves	Lung, blood vessels, eye, mast cells	Cerebellum, hippocampus
Low expression	Lungs, pancreas	Other brain regions	Adipose tissue, adrenal gland, brain, kidney	Thyroid, most of brain, adrenal gland, spleen, liver, kidney, heart

Table 1 Distribution and expression of adenosine receptors [4]

All of the four adenosine receptors stimulate or inhibit the activity of the Adenylate Cyclase (AC). [4] A_1AR and A_3ARs inhibit the activity of AC via $G_i/G_0/G_q$ –proteins which results in decreasing levels of cAMP. A_{2A}AR - and A_{2B}AR are coupled to G_s subunits and activate AC, which induces increased levels of cAMP and activation of Protein kinase A (PKA). [9] Furthermore the A_3ARs cause a $G_{\beta\gamma}$- dependent activation of Phospholipase C (PLC) with a succeeding Ca^{2+}-signal and activation of MAP-Kinase signalling. [10] AC and PLC are not the only effector mechanisms associated with the activation of ARs. Adenosine is able to activate phosphoinositide-3-kinase (PI3K), mitogen-activated protein (MAP) kinases and extracellular receptor signal-induced kinase (ERK). [1]

The A_{2B}AR displays the lowest affinity (K_i>1μM) of the four receptor subtypes to native adenosine. A_1AR and A_{2A}AR demonstrate the highest affinity to adenosine while A_3AR has intermediate affinity. [1]

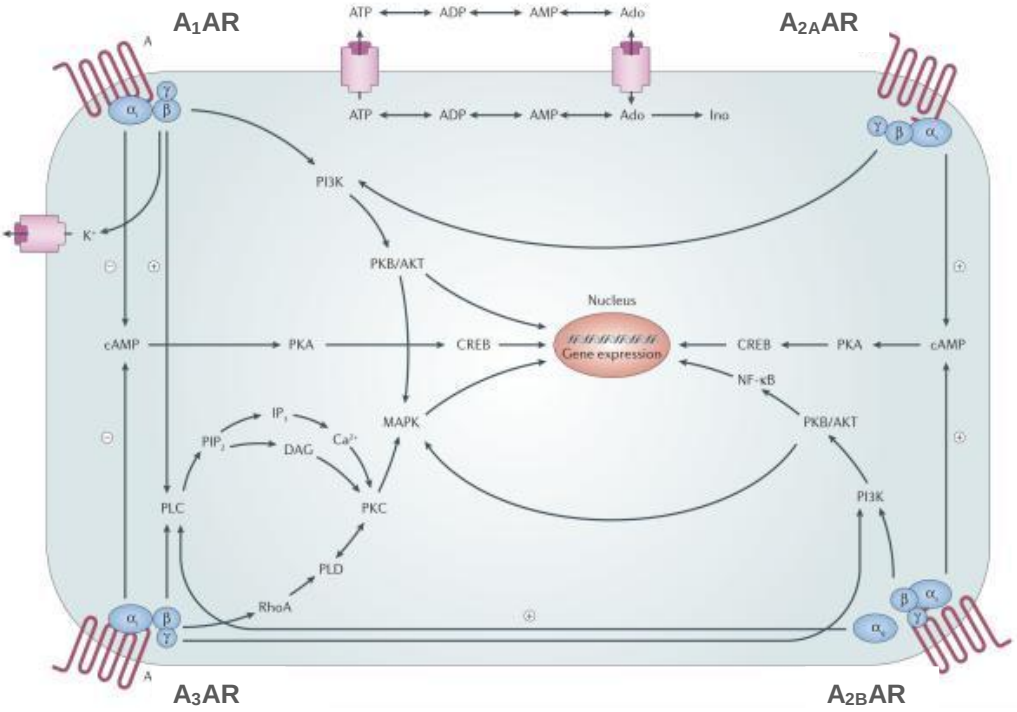

Figure 2 Adenosine receptor signaling pathways [2]

The regulation of many physiological functions by activation of A_1AR, A_{2A}AR, A_{2B}AR, A_3AR, makes these receptors promising targets in a great variety of pathophysiological conditions including “cerebral and cardiac ischaemic diseases, sleep disorders, immune and inflammatory disorders and cancer.” [2]

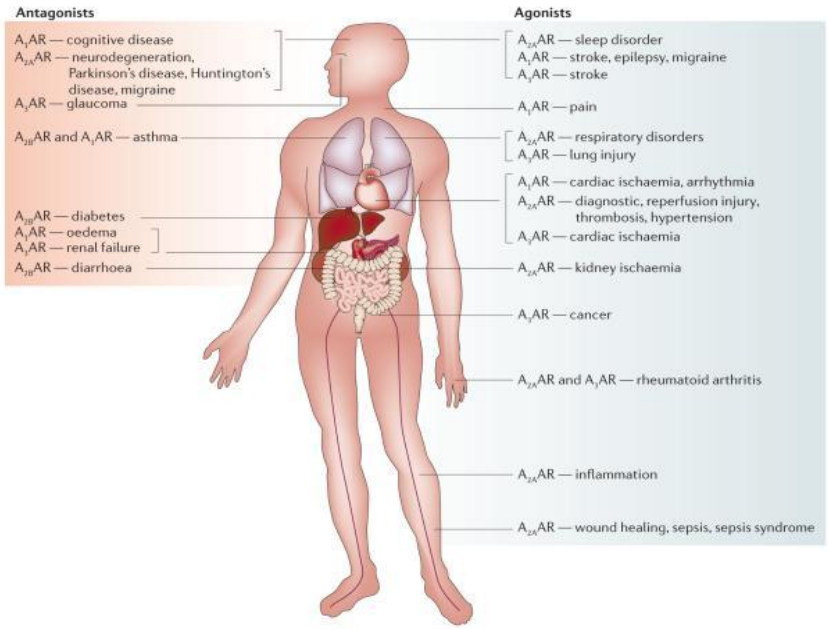

Figure 3 Novel disease targets for selective adenosine receptor ligands [2]

1.1.1 Adenosine A_1 - Receptor

The A_1AR couples to G_i, inhibits the activity of AC and activates PLC. Additionally it activates K^+ channels and inhibits Ca^{2+} channels. A_1AR is expressed ubiquitous throughout the entire body with the highest levels detected in the brain. [11] It influences sleep promotion and protects embryos against hypoxia. [2, 12] Activation of A_1AR also results in effects within the cardiovascular system. It reduces the heart rate, the atrial contractility and the stimulatory response to catecholamines on the heart. Furthermore, activation of A_1AR protects tissues against hypoxia or ischaemia and a recently developed antagonist (FR194921) showed effects in the therapy of dementia and anxiety disorders. [2]

Selectivity of agonists for A_1AR is achieved by substitution at the adenosine N_6-position and selectivity of antagonists by modification of xanthines. [2]

1.1.1.1 Adenosine A_1 -Receptor-Antagonist

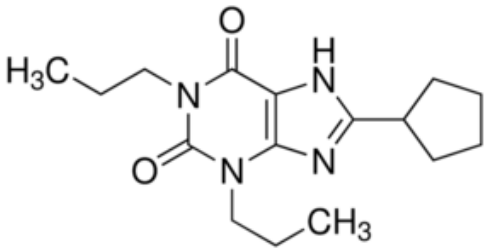

Figure 4 DPCPX (1,3-dipropyl-8-cyclopentyl xanthine) [13]

For almost one hundred years of research the chemical core-structure remained unchanged until the methyl substituents were replaced by n-propyl chains and a cyclopentane was installed at the C_8 -position. [14] This led to the discovery of 1,3-dipropyl-8-cyclopentyl xanthine and showed to be selective for rat A_1AR and less selective at the human A_1AR. [15]

More A_1AR-Antagonists: KW3902 (3-noradamantyl-1,3-dipropylxanthine), BG9928 (3-(4-(2,6-dioxo-1,3-dipropyl-2,3,6,7-tetrahydro-1H-purin-8-yl)bicyclo[2.2.2]octan-1-yl)propanoic acid), SLV320 (4-(2-phenyl-7H-pyrrolo[2,3-d]pyrimidin-4-ylamino)cyclohexanol) [14]

1.1.2 Adenosine A_{2A}-Receptor

Research indicates involvement of A_2AR in the regulation of the central nervous system, interaction with dopamine D_2 receptors and suggests A_2AR-antagonists in the treatment of Parkinson's disease. Furthermore, the A_2AR takes part in the regulation of inflammatory and immune responses. Studies assume A_2AR to play an important role in the elimination and limitation of prolonged inflammation. [2]

1.1.2.1 Adenosine A_{2A} -Receptor-Antagonist

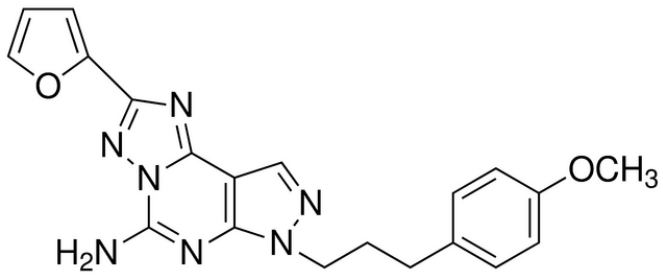

Figure 5 SCH 442416 (5-amino-7-[3-(4-methoxyphenyl)propyl]-2-(2-furyl)pyrazolo[4,3-e]-1,2,4-triazolo[1,5-c]pyrimidine) [16]

This nonxanthine-derivative shows high selectivity for the human A_{2A}AR and has been used ^{11}C-labeled as a tool for PET studies with a k_i=0,048nM. [1]

More A_{2A}AR-Antagonists: Caffeine, Theophylline, KW-6002, SCH-442416, ZM-241,385 [1]

1.1.3 Adenosine A_{2B}-Receptor

The A_{2B}AR couples to G_s/G_q under high concentrations of extracellular adenosine and stimulates AC and PLC. [4] Studies suggest involvement of A_{2B}AR in vasodilatation, hypoxia and inhibition of cardiac fibroblast functions. [2] Furthermore, A_{2B}AR could also be a future target in the treatment of asthma and chronic obstructive pulmonary disease. [17]

1.1.3.1 Adenosine A_{2B} - Receptor - Antagonist

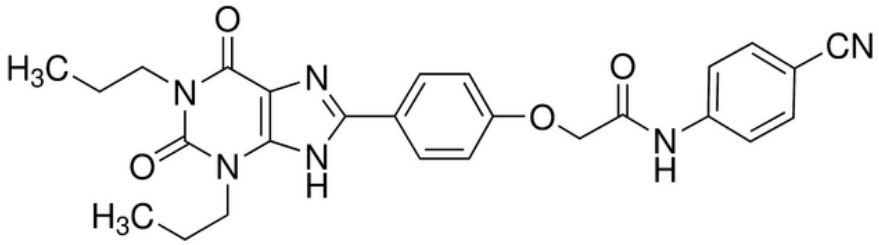

Figure 6 MRS1754 (N-(4-cyanophenyl)-2-[4-(2,3,6,7-tetrahydro-2,6-dioxo-1,3-dipropyl-1H-purin-8-yl)-phenoxy]acetamide) [18]

MRS 1754 is a para-cyano-anilide derivative and shows high affinity for the A_{2B}AR with a k_i=1.97 nM. [19]

1.1.4 Adenosine A_3-Receptor

The A_3AR subtype couples to G_i and so inhibits the AC, which activates the PLC-pathway through the β- and χ- subunit. The A_3AR is highly distributed in the lungs, liver and immune cells such as neutrophils and macrophages. In a lower density the A_3AR is expressed in the heart and the brain. [20] The A_3AR can be detected in almost all brain areas but in a much lower density compared to other AR subtypes. Additionally it responds to micromolar concentrations while other subtypes are activated by nanomolar concentrations. [21] It is involved in cytoprotective functions comprising anti-inflammatory, anticancer and cardioprotective effects. Recent studies discovered preconditioning and protection of cardiac myocytes against ischaemic damage and apoptosis by A_3AR. Further studies are implemented for the development of potential antiglaucoma agents. [20]

Studies showed increased expression of A_3AR in human lung biopsies of patients with asthma or COPD. Effects of A_3AR activation on human eosinophils comprise the release

of superoxide anion, inhibition of degranulation and additionally inhibition of chemokine-induced migration. Furthermore, preclinical studies assume that A_3AR is involved in the progression of chronic inflammatory diseases of the airways. [17]

A_3AR expression was discovered in several tumor cell lines including “astrocytoma, HL-60 leukemia, B16-F10 and A378 melanoma, human Jurkat T-cell lymphoma and murine pineal tumor cells”, while the distribution of A_3AR in non-pathophysiological tissues was low. [22] Further studies suggest an increased expression of A_3AR in various malignancies. In solid tumors overexpression of the A_3AR was discovered and studies assume that A_3AR expression level is associated with disease severity. Studies with primary thyroid cancer tissue revealed high levels of A_3AR while non-pathological thyreoid tissue samples show no expression of A_3ARs. Receptor binding values were examined in colon carcinoma tissue and revealed an increased binding value in comparison to healthy colon mucosa. [22]

1.1.4.1 Adenosine A_3-Receptor-Antagonist

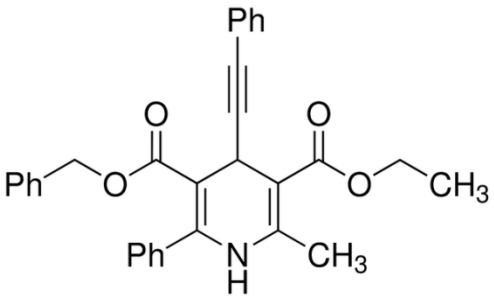

Figure 7 MRS 1191 (1,4-Dihydro-2-methyl-6-phenyl-4-(phenylethynyl)-3,5-pyridinedicarboxylic acid, 3-ethyl 5-(phenylmethyl) ester) [23]

MRS 1191 is a 1,4-dihydropyridine-derivative which was discovered through library screening and identified as a weak A_3AR- antagonist with k_i=31 nM. [20]

1.1.4.1 Radiolabelled Antagonists for A_3AR

[^{18}F]FE@SUPPY (2,4-diethyl-3-(ethylsulfanylcarbonyl)-6-phenylpyridine-5-carboxylate) [24]

[^{18}F]FE@SUPPY:2 (5-ethyl 2,4-diethyl-3-((2- [18F]flourethyl)sulfanylcarbonyl)-6-phenylpyridine-5-carboxylate) [24]

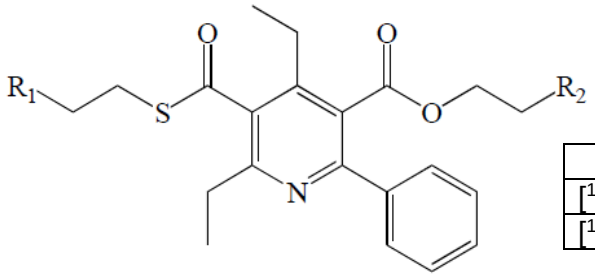

	R_1	R_2
[^{18}F]FE@SUPPY	-H	-^{18}F
[^{18}F]FE@SUPPY:2	-^{18}F	-H

Figure 8 Structural differences in [^{18}F]FE@SUPPY and [^{18}F]FE@SUPPY:2 [24]

This structure was discovered as an antagonist with a fluorethylester-moiety and called compound number 7. [25] It was named [^{18}F]FE@SUPPY after labelling it with [^{18}F] and shows affinity for the A_3AR (ki= 4.22 nM). [26] It is a derivate of the chemical family of 3,5 – Diacyl-2,4-dialkylpyridines. [24]

[^{18}F]FE@SUPPY:2 binds ^{18}F in contrast to [^{18}F]FE@SUPPY at the thioester moiety. Similar effects on the A_3AR are expected. [24]

For more details, please refer to chapter 2.2.4. Radiosynthesis of [^{18}F]FE@SUPPY and [^{18}]FE@SUPPY:2.

[^{125}I]-AB-MECA

[^{125}I]-4-aminobenzyl-5'N-methylcarboxamidoadenosine shows high affinity for A_3AR with k_D=0.6 nM and additionally affinity for A_1AR. By inhibition of A_1AR it is possible to selectively detect A_3AR. [27]

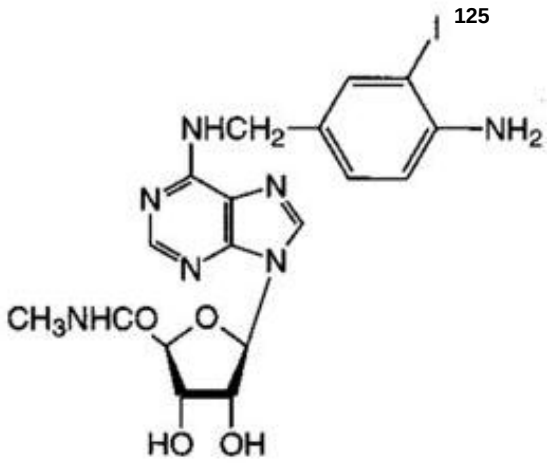

Figure 9 [^{125}I]-AB-MECA [28]

1.2 Substrate-Receptor Interaction

A drug is made effective by substrate-receptor binding. The mathematical description is based on the law of mass action and the Michaelis-Menten-Kinetik. [29]

$$E + S \rightleftharpoons ES \rightleftharpoons E + S$$

The enzyme (E) is reversibly binding the substrate (S) and the complex of enzyme-substrate results in catalytic enzyme-metabolit-complex (EM), which disaggregates into the enzyme (E) and the metabolite (M). [29]

Transferred to binding of receptor-substrate the equation results in:

$$R + D \rightleftharpoons RD \rightleftharpoons RD_M \underset{k_{-1}}{\overset{k_{+1}}{\rightleftharpoons}} R + D_M$$

R: Receptor

D: Drug

RD: Receptor-Drug-Complex

D_M: enzymatic modified Drug

k_{+1}: rate constant of the forward chemical process

k_{-1}: rate constant of the backward chemical process

$$\frac{[R] \times [P]}{[RP]} = \frac{k_{+1}}{k_{-1}} = k_D$$

The steady state reflects the binding equilibrium between the receptor and the ligand. Thereforem, k_D expresses the affinity of a ligand or the disposition of a receptor-ligand complex to dissociate. [30] The IC_{50} is defined as the concentration of an antagonist, which is needed to accomplish 50% inhibition. [29] This parameter is converted with the equation of Cheng & Prusoff to the k_i, the equilibrium inhibitor constant, determining the potency of a compound as inhibitor. [30]

$$K_i = \frac{IC_{50}}{1 + \frac{[L]}{K_D}}$$

1.3 Radioactivity

In 1886 Henry Becquerel discovered radiation emitted by uranium materials. The photographic plates he used for his experiments were blackened when being in contact with the minerals in the absence of light. Two years later Marie Curie found differences in the radioactivity of uranium and uranium minerals and came to the conclusion that these minerals contain other radioactive elements. [31] Approximately 3000 nuclides have been discovered by now, most of which are unstable. These unstable nuclides decay by spontaneous fission, α-decay, β-decay, γ-ray emission, electron capture or isomeric transition to reach stability. The neutron-to-proton ratio (N/Z) is one criterion of stability and so radionuclides decay to reach the N/Z of the closest potentially stable nuclide. [32]

1.3.1 Radioactive decay

1.3.1.1 Spontaneous Fission

The breaking down of a heavy nucleus into two fragments, generally in the ratio of 60:40, is called Fission. During this process two or three neutrons are emitted with an average energy of 1.5 MeV and a release of ~200 MeV. Fission in heavy nuclei happens spontaneously or by bombarding with energetic particles. [32]

1.3.1.2 α-decay

The α-decay usually takes place in heavy nuclides e.g. Uranium or Radon by α-particle emission. $^{4}_{2}\mathbf{He}$ is emitted by α-decay and so the atomic number of the parent nuclide is reduced by two Units and the mass number by four Units. [32]

Example of α-decay:

$$^{235}_{92}\mathbf{U} \rightarrow {}^{231}_{90}\mathbf{Th} + {}^{4}_{2}\mathbf{He}^{2+}$$

1.3.1.3 β^--decay

A “neutron rich” nucleus, which reveals a higher N/Z -ratio in contrast to the stable nucleus, decays by β^--particle emission along with the emission of an antineutrino. The antineutrino ($\bar{\nu}$) is an entity virtually without mass and no charge and preserves the energy in the decay. During the β^--decay a neutron decays into a proton and a β^--particle. [32]

$$\mathbf{n \rightarrow p + \beta^- + \bar{\nu}}$$

Emission of the β^--particle is happening with differing energy from zero up to the decay energy. This decay energy is also called transition energy and describes the difference in energy between the parent and the daughter nuclides. The antineutrino removes the difference between the β^--particle energy and the decay energy. After β^--decay the atomic number of the daughter nuclide is increased for one Unit compared to the mother nuclide. [32]

Example of β^--decay:

$$^{99}_{42}\mathbf{Mo} \rightarrow {}^{99m}_{43}\mathbf{Tc} + \mathbf{\beta^-} + \bar{\nu}$$

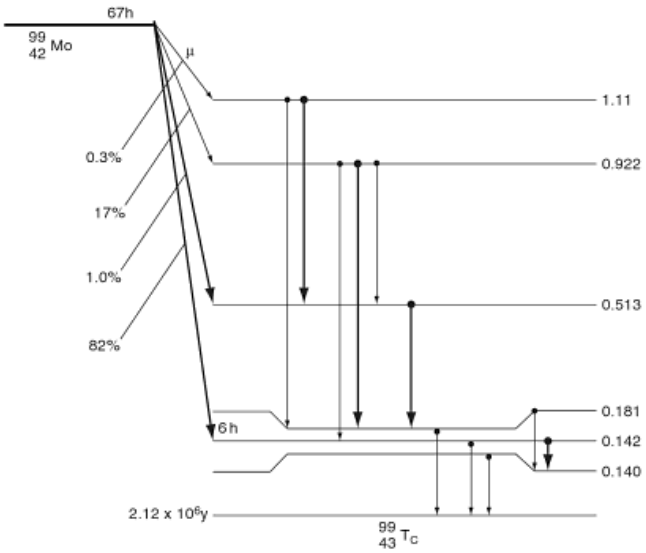

Scheme 1 Decay scheme of β^--decay [33]

1.3.1.4 β^+ -decay

"Neutron-deficient" or "proton rich" nuclei, which reveal a N/Z- ratio less than that of the stable nuclei, decay by β^+-particle emission. This results in the emission of a neutrino (v), which is the mirror particle of an antineutrino. [32]

$p \rightarrow n + \beta^+ + v$

After emission of the β^+-particle, the atomic number of the daughter nuclide has been reduced for one Unit. [32]

Example for β^+ -decay:

$$^{18}_{9}F \rightarrow {}^{18}_{8}O + \beta^+ + \nu$$

The β^+-particle can be emitted with energy between zero and decay energy and the neutrino takes away the difference between decay energy and β^+-energy. Within the β^+-decay a mass equivalent of two electrons is created by the conversion of a proton to a neutron and 1.02 MeV is required to produce these two particles. In regard to this fact, the emission takes place only when the energy distinction between the parent and the daughter nuclides is equal to or greater than 1.02 MeV. [32]

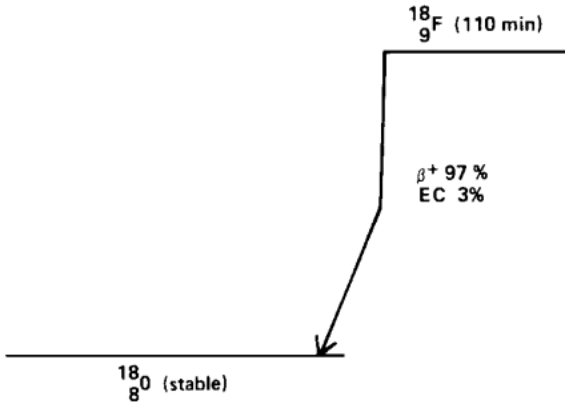

Scheme 2 Decay scheme of β^+ -decay [32]

1.3.1.5 Electron capture (EC) or ε -decay

Like the β^+ -decay, EC-decay occurs in “proton-rich” nuclides. Here an electron, most commonly from the K-Shell, is captured, which transforms a proton into a neutron and emits a neutrino. The K-shell electrons are captured due to the vicinity to the nucleus. The energy difference between the parent and the daughter nuclides is most of the time, but not implicitly less than 1.02 MeV. [32]

$$^{67}_{31}\mathbf{Ga} + {}^{\mathbf{0}}_{\mathbf{-1}}\mathbf{e}^{-} \rightarrow {}^{67}_{30}\mathbf{Zn} + \boldsymbol{\nu_e}$$

1.3.1.6 Isomeric- transitions

The nucleus can remain in an upper excited state above the ground state. The decay to the lower excited state is called isomeric transition and the difference between the energy states turns out as γ rays. Excited states with a long living nature are called metastable states. ^{99m}Tc is a metastable γ ray emitter and decays by isomeric transition. [32]

1.4 Production of Radionuclides

Radiopharmaceuticals are composed of a radionuclide and a pharmaceutical component. Radionuclides, which are used in nuclear medicine, are usually produced artificially. In the meantime, production of more than 2700 radionuclides has been accomplished in a cyclotron, a reactor, a neutron generator or a linear accelerator. [32]

1.4.1 Reactor-produced radionuclides

Fission is induced in a nuclear reactor, which is build up of fuel rods made of fissile material (e.g. ^{235}U, ^{239}Pu). By fission, a heavy nucleus breaks up into two fragments of approximately equal mass and two or three neutrons are released with energies of about 1.5 MeV. Furthermore, concomitant energy of 200 MeV is set free and has to be taken off by heat exchangers. [32] Reactor-generated neutrons can be utilised to produce radionuclides by neutron activation. The target nuclei which is placed in the reactor core has the ability to capture neutrons and to create a radioactive product nuclei through (*n,p*) and (*n,γ*) reactions. Within the (*n,p*) reaction, a neutron is captured by the target nucleus and a proton is released, which transforms the target to a different chemical element. The resulting product is carrierfree and demonstrates high specific activity. Within the (*n,γ*) reaction, the target nucleus is transformed into an excited state of the product nucleus. During deexcitation, this product nucleus emits a *γ*-ray. The products produced by (*n,γ*) reaction are not carrier-free as the chemical element is the same as the target material. [34]

Examples for reactor-produced radionuclides: ^{99}Mo, ^{131}I, ^{133}Xe [32]

1.4.2 Cyclotron-produced radionuclides

Furthermore, the production of radionuclides can be implemented by using a cyclotron. A cyclotron accelerates charged particles to an adequate energy to finally surmount the repulsive charge enclosing a positively charged nucleus, when the particle is directed towards a target nucleus. The cyclotron is build up of two semi-circular cylinders called “dees”. These dees are situated in a magnetic field and are separated by a gap. They are connected to an electrical system, which changes the electrical potential on each dee. Therefore, a charged particle moves to the dee which has the opposite charge. This results in an acceleration of the particle into the dee in a semi-circular route. By crossing through the first dee, the charge of each dee is changed to the opposite charge. The first dee then holds the same charge as the particle and for this reason the particle is repelled. The opposite dee carries now the opposite charge and the particle is consequently pulled and accelerated across the gap. By repeating this process, the particle acquires energy while the radius of the path within the dees is increasing. When carrying enough energy to overcome the electrical field around the nucleus of a target atom, the charged particle is directed to a target. [35]

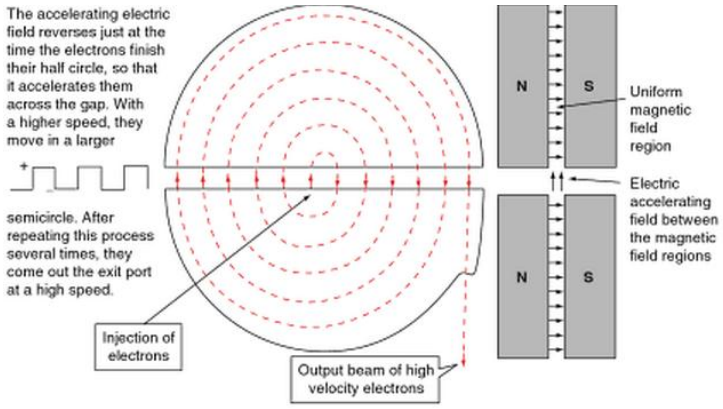

Figure 10 Production of radionuclides with cyclotron [33]

Thereupon, irradiation of the target nuclei by the accelerated particles takes place and the nuclear reaction occurs. The incident particle may exit the nucleus after the nuclear reaction and leave some of its energy in it. Alternatively, it can be entirely absorbed by the nucleus, depending on the particle`s energy. A nucleus with excitation energy is created and the energy is eliminated by particle emission, which is succeeded by γ-ray emission. Several nucleons are emitted from the irradiated target nucleus, which depends on the energy saved by the incident particle, resulting in the formation of different nuclides. [32]

Examples for cyclotron-produced nuclides: ^{111}In, ^{201}Tl, ^{11}C, ^{13}N, ^{15}O, ^{18}F [32]

1.4.3 Generator production

The radionuclide-generators employ parent- and daughter nuclides. The parent isotope is a radioactive nuclide which is used with the purpose to gain a new radionuclide by nuclear decay, called daughter isotope. Parent and daughter are both present in the generator until the removal of the daughter isotope. The ^{99}Mo/^{99m}Tc generator is the most frequently used generator in nuclear pharmacy. ^{99}Mo has a half-life of 66.7 hours and decays by β- and γ-decay. It decays 86% of the time to ^{99m}Tc, which shows a half-life of 6.02 hours and decays by isomeric transition. ^{99}Mo is acidified and adsorbed as MoO_4^{2-} on a generator column packed with alumina (Al_2O_3), which holds a positive charge. After the decay of ^{99}Mo, the daughter nuclide ^{99m}Tc is present as $^{99m}TcO_4^-$, which can be eluted by a saline solution into the evacuated vial. [35]

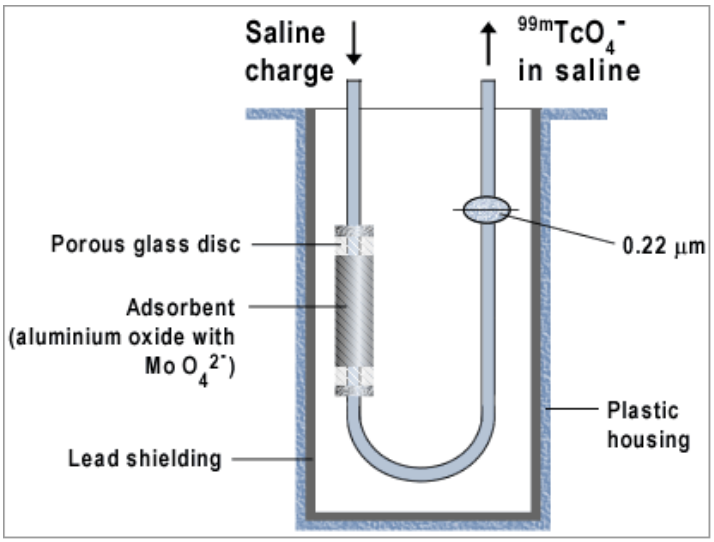

Figure 11 ^{99}Mo/^{99m}Tc generator [36]

1.5 Nuclear imaging

Nuclear medicine uses internally administered radioactive substances called radiotracer. These radiotracers are substances which are labelled with radioactive elements by chemical synthesis. Images of the internal distribution of radioactivity can be produced with specialized instrumentation. The images represent a mirror of the compound of interest and are compared with known distributions in diverse disease states. [37] Radioligands have to show high affinity, high selectivity and low unspecific binding to receive imaging with high quality. [38]

1.5.1 Single-photon emission computed tomography (SPECT)

In SPECT single photon emitters are used, which emit one γ-ray photon with each decay moment. After administration of the radiopharmaceutical, imaging devices detect and record the emitted γ-rays. Due to safety concerns, the rate of emission is very low and so data collection takes a relatively long time compared to other methods e.g. X-Ray CT. γ- Rays are detected by the gamma camera, often called Anger camera, which contains a system of detection hardware on the opposite side of the collimator. The image of the radiopharmaceutical distribution is created by a collimator, which consists of a thick sheet of heavy material e.g. lead and is perforated by long thin channels. The collimator generates an image of rays, which travel in the direction of the channels. After transition through the collimator, the gamma ray strikes the first element of the detection device,

called scintillator. This scintillator consists of a crystal material which utilises energy of the γ-rays to produce optical-wavelength photons. The photons are registered by a collection of photomultiplier tubes (PMTs), which produce a cascade of electrons and as a result a measurable electrical current. Electronic devices detect the current and register the incidence of the event. Therefore, two-dimensional spatial coordinates of the gamma-ray event relative to the face of the camera can be calculated. The events are tallied in a histogram, which serves as a projection image of the object. [39]

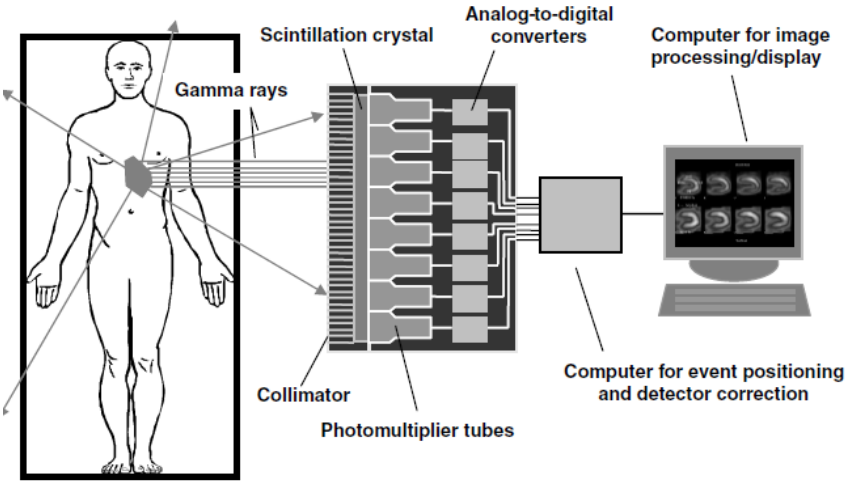

Figure 12 Schematic diagram of a conventional gamma camera used in SPECT [39]

1.5.2 Positron emission tomography (PET)

PET uses in contrast to SPECT positron-emitting radionuclides instead of single-photon emitters. The decay of a positron-emitting isotope results in the emission of two gamma rays that travel from each other in almost opposite directions. [39] The decay is induced by the annihilation of a positron of the radionuclide and an electron in the medium, which leads to the appearance of two 511 keV annihilation photons. [32] The patient is surrounded by a ring of detectors or a single Anger camera can be used to register the γ-rays. The data is translated into projections and filtered back-projection is accomplished. The advantage of using PET instead of SPECT lies in the use of the radionuclides. ^{11}C, ^{13}N, ^{15}O and ^{18}F are isotopes of elements which can be found naturally in organic molecules. Furthermore, the radiopharmaceutical synthesis is simplified and the demand to use molecules with only as small changes as possible is fulfilled. Due to the short half-lives of the radionuclides, measurements of a series of studies within one day without background activity of prior injections can be acquired. [37]

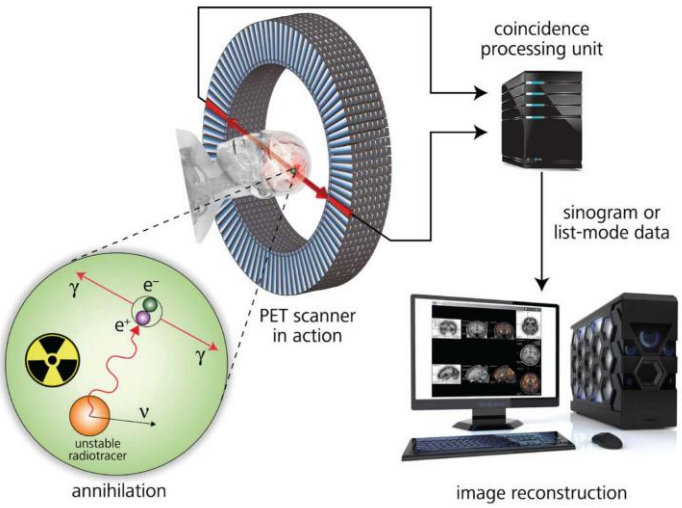

Figure 13 Standard process for generating PET imaging [40]

1.5.3 Autoradiography

Autoradiography describes a tool to map the distribution of a radiolabelled ligand in thin sections of tissue. [41] It is a collection of several techniques with certain attributes in common. The most commonly used methods of autoradiography comprise *in vivo* labelling of laboratory animals and *in vitro* labelling of tissue cryosections. By performing *in vivo* autoradiography, a radiolabelled chemical is administered to a specimen, which is later sacrificed and sectioned. The comprehensive image of the anatomy provides information about the distribution of the radiolabelled ligand within the specimen. *In vivo* autoradiography is accomplished to evaluate toxicity, distribution in the body and fetal transmission. [42] *In vitro* autoradiography is performed on tissue sections and distribution of drug receptors can be made visible. It also allows evaluation of binding sites and information about drug displacement can be obtained. [41]

2. Materials and Methods

2.1. Materials

2.1.1. Cyclotron Equipment

[^{18}F]Fluoride	^{18}O(p, n)^{18}F nuclear reaction in GE PETtrace cyclotron (16.5 MeV protons)

Enriched $H_2{}^{18}O$	Rotem Medical (Dimona, Israel)

2.1.2. Production of [^{18}F]Fluoride

Kryptofix 2.2.2. (4.7.13.16.21.24-Hexaoxa-1,10-diazabicyclo[8.8.8]-hexacosane)	Merck, Germany
K_2CO_3	Merck, Germany
Chromafix® 30 PS-HCO3 Cartridges	Macherey-Nagel, Düren, Germany
1mL Grad V-Vials	Wheaton (Millville, USA)
PTFE silicone septa	Wheaton Science Products (Millville, USA)

2.1.3. Radiosynthesis and HPLC Equipment

GE TRACERlab Fx_{FN} synthesizer	GE Healthcare Systems
semi-preparative reversed-phase HPLC system	column: Merck Chromolith® SemiPrep RP-18e, 100x10mm, mobile phase: acetonitrile/water/acetic acid 60/38.8/1.2
HPLC Analyses	Merck LiChrospher 100-250 RP-18e column (5µm, 250mm x 4.6mm); Merck-Hitachi LaChrom gradient;L-6200 gradient pump, a Merck-Hitachi L-7400 UV detector (254nm); lead-shielded NaI radiodetector; Berthold Technologies; Bad Wildbad, Germany
TOS@SUPPY	Department of Drug and Natural Product Synthesis, Dr. Karem Shanab, Faculty of Life Sciences, University of Vienna
TOS@SUPPY:2	Department of Drug and Natural Product Synthesis, Dr. Karem Shanab, Faculty of Life Sciences, University of Vienna

2.1.4. Solvents, Buffers

Acetonitrile	Merck (Darmstadt, Germany)
Aqua purificata	AKH Vienna
Isopentan	Merck, Germany
0,9% normal saline solution	BBraun, Austria
PBS Buffer ph=7.4	Morphisto, Germany
Tris(hydroxymethyl)-aminomethane	Sigma Pharma, Austria

2.1.5. Dissection of laboratory rats

Laboratory rats	Abteilung für Biomedizinische Forschung, Medical University of Vienna
Water	VWR, Austria
Greiner Tubes	Greiner, Austria

2.1.6. Sectioning of organs

Mikrotom-Kryostat	Microm Cryo HM 560 M, AKH Vienna
Frozen section medium	Richard Allen Neg-50 Frozen Section Medium
Super Frost Slides	Thermo Scientific, Germany

2.1.7. Antagonists

DPCPX	Sigma-Aldrich Chemie, Germany
MRS 1191	Sigma-Aldrich Chemie, Germany
MRS 1754	Sigma-Aldrich Chemie, Germany
SCH 442416	Sigma-Aldrich Chemie, Germany

2.1.8. Agonists

[^{125}I]-AB-MECA	Perkin Elmer, Boston

2.1.9. Autoradiography

PAP Pen	Thermo Scientific, Germany
Cyclone Plus Phosphorimager	Perkin Elmer, Boston
Eppendorf Tubes 1 ml	Eppendorf, Germany
Eppendorf Pipettes 0.5 µl – 1000 µl	Eppendorf, Germany

2.2. Methods

2.2.1. Dissection of laboratory rats

Male rats of unknown race have been sacrificed by inhalation of CO_2. Dissection started at the cranial area by making an incision starting from the top of the vertebra along to forehead. The surface was cleaned of fur, skin and muscles with a scalpel.

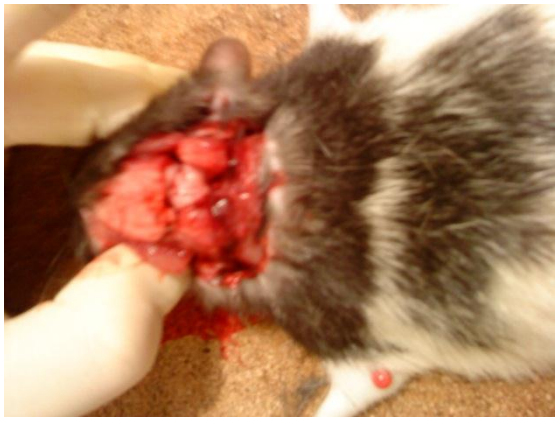

Figure 14 Exposed cranial region with musculus masseter and musculus auricularis [43]

The cervical vertebrae were cut with a scissor and the bone fragments removed with a forceps. Then the top of the scissor was placed slightly through the foramen magnum at the base of the skull and with using pressure the occipital bone was cracked. The cranium was cut with a scissor and the remaining pieces of the bone picked away with a forceps until the brain was fully exposed. Finally the spinal cord and the medulla oblongata were stripped off. [44]

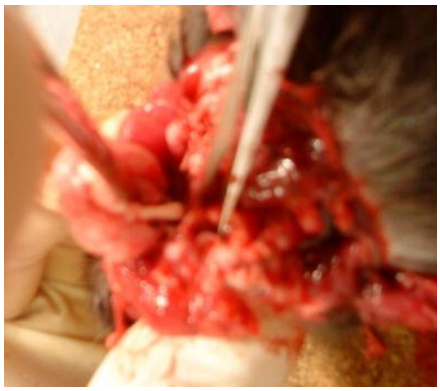

Figure 15 Spinal Cord and Medulla oblongata [43]

The brain was removed with a spoon and cleaned in a Greiner tube with 10 ml of 0.9% normal saline solution and afterwards in a Greiner tube with 10 ml cold water. After freezing approximately two minutes in isopentane from -40°C to -45°C with the aim to freeze the organ as fast as possible to eliminate ice crystal formation, it was cooled in a Greiner Tube surrounded by dry ice. This purification process was also performed with the later removed organs.

After dissection of the cranial area the rat was turned over and prepared for removing the inner organs.

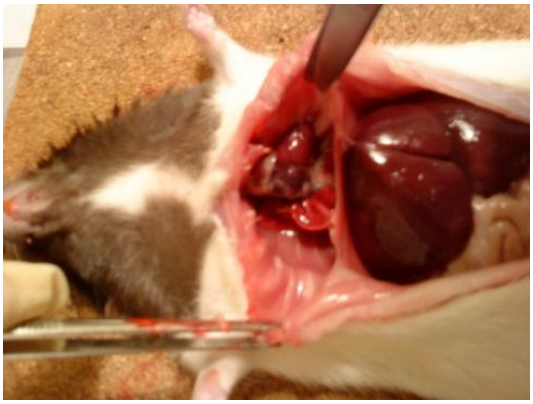

Figure 16 Heart, lungs, diaphragm, liver and duodenum of exposed laboratory rat [43]

An incision was made into the abdominal wall with a scissor and afterwards carefully cut through with a scalpel to not damage the underlying structures. The Aorta, the Ductus Botalli and the Arteria pulmonalis were cut to finally remove the heart.

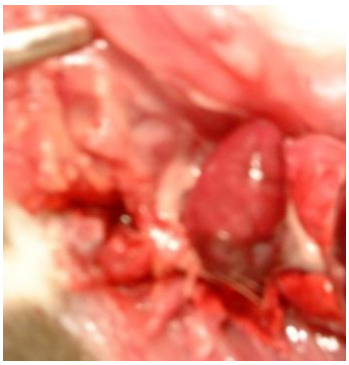

Figure 17 Exposed thoracic region: Heart, coronary blood vessels and lungs [43]

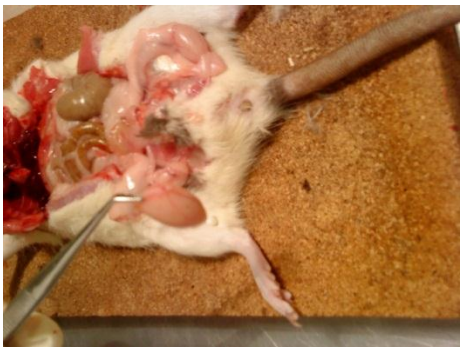

Figure 18 Scrotum and testis [43]

The scrotal sac was cut with a scissor. The vas deferens was separated and testes removed with a scissor. The organs were immediately stored at -80°C.

2.2.2. Cryo-Sectioning of Organs

Figure 19 Microm Cryo HM 560 M [43]

The organs were adjusted to -20°C before performing sectioning in the Microm Cryo HM 560 M cryostat and therefore placed into the refrigerator with the set temperature. The organ was mounted the next day with frozen section medium on the cryocassette and sectioned into 30 µm thick slices. Sections were attached on Superfrost adhesive slides and were stored in a refrigerator with a set temperature of –40°C.

Figure 20 Rat brain placed on frozen section medium [43]

The chosen temperature of the chamber and the blade differed between organs when accomplishing sectioning.

Organ	Temperature – Chamber	Temperature- Blade
Brain	-10°C	-10°C
Heart	-20°C	-20°C
Testes	-10°C	-20°C

Table 2 Temperatures to implement optimal cryo-sectioning

2.2.3. Production of [^{18}F]fluoride

The production of [^{18}F]fluoride was performed in the GE PETtrace Cyclotron. $H_2{}^{18}O$ (>98%) was irradiated with a proton beam and thereby the ^{18}O (p,n)^{18}F nuclear reaction was accomplished in a silver target. The irradiation process was monitored by a computer system and irradiation stopped after attaining a determined activity. Afterwards, the product was transferred into a vial. The solution containing [^{18}F]fluoride was passed through an anion exchange cartridge to remove $H_2{}^{18}O$. [^{18}F]fluoride remained at the cartridge and was eluted with a solution of potassium carbonate (4.5mg, 32.6µmol) and Kryptofix 2.2.2 (20mg, 53,2µmol) in acetonitrile/water (70:30 v/v%). [^{18}F]fluoride moved into the organic phase and the solution was heated to 100°C. The remaining water had to be azeotropically removed and consequently 1 ml acetonitrile was added twice under a stream of nitrogen gas over a period of 10 minutes. The dried [^{18}F]fluoride was then cooled to room temperature.

2.2.4. Radiosynthesis of [^{18}F]FE@SUPPY and [^{18}]FE@SUPPY:2

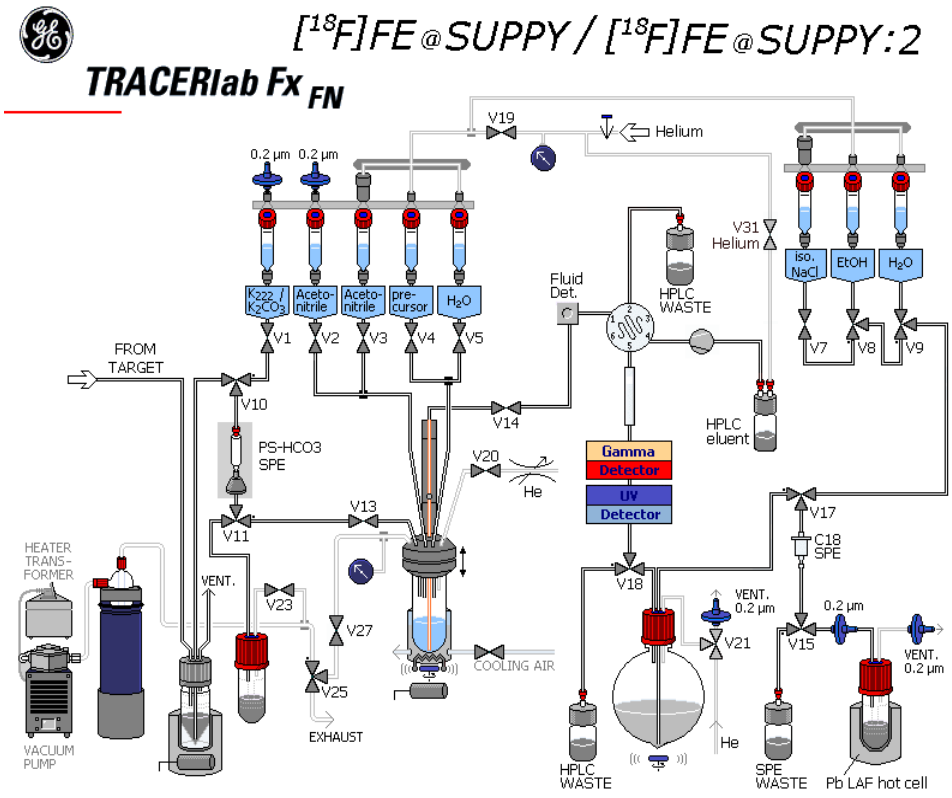

Figure 21 Overview GE TRACERlab Fx$_{FN}$ synthesizer [24]

The radiosynthesis of [^{18}F]FE@SUPPY and [^{18}]FE@SUPPY:2 was performed on a GE TRACERlab Fx$_{FN}$ synthesizer. A solution of 20mg TOS@SUPPY or TOS@SUPPY:2 in 1 ml acetonitrile was prepared prior to the synthesis start. The solution was heated for 20 minutes at 75°C. 500µl of TOS@SUPPY or 1ml TOS@SUPPY:2 was added to the cooled and dried [^{18}F]fluoride. The vial was placed on the designated spot and connected to the corresponding tubing. When starting the synthesis, the fluid was delivered to the injector of the semi-preparative reversed-phase HPLC system. The injector automatically switched from “load” to the “inject” position after being triggered by the fluid detector. The desired peak was cut manually and was transferred over a C18plus SepPak$^{@}$ in a stream of helium. The product was eluted with 2.5 ml ethanol via sterilfilter into the vial. [24]

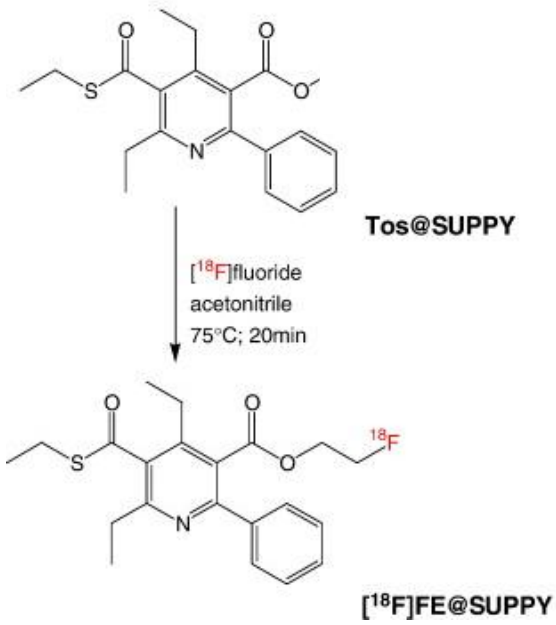

Figure 22 Radiosynthesis of [18F]FE@SUPPY [26]

Afterwards, HPLC was used to determine retention time and peak area. Radioactivity rate was measured.

Calibration curve of [18F]FE@SUPPY and [18]FE@SUPPY:2

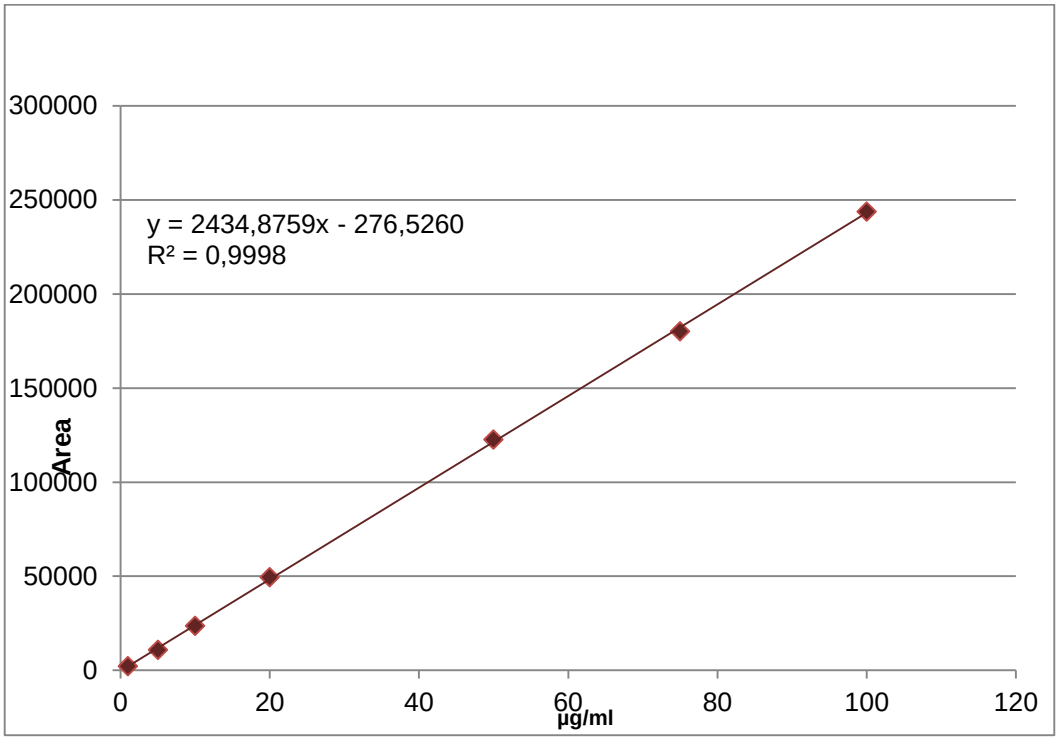

Figure 23 Calibration curve of FE@SUPPY

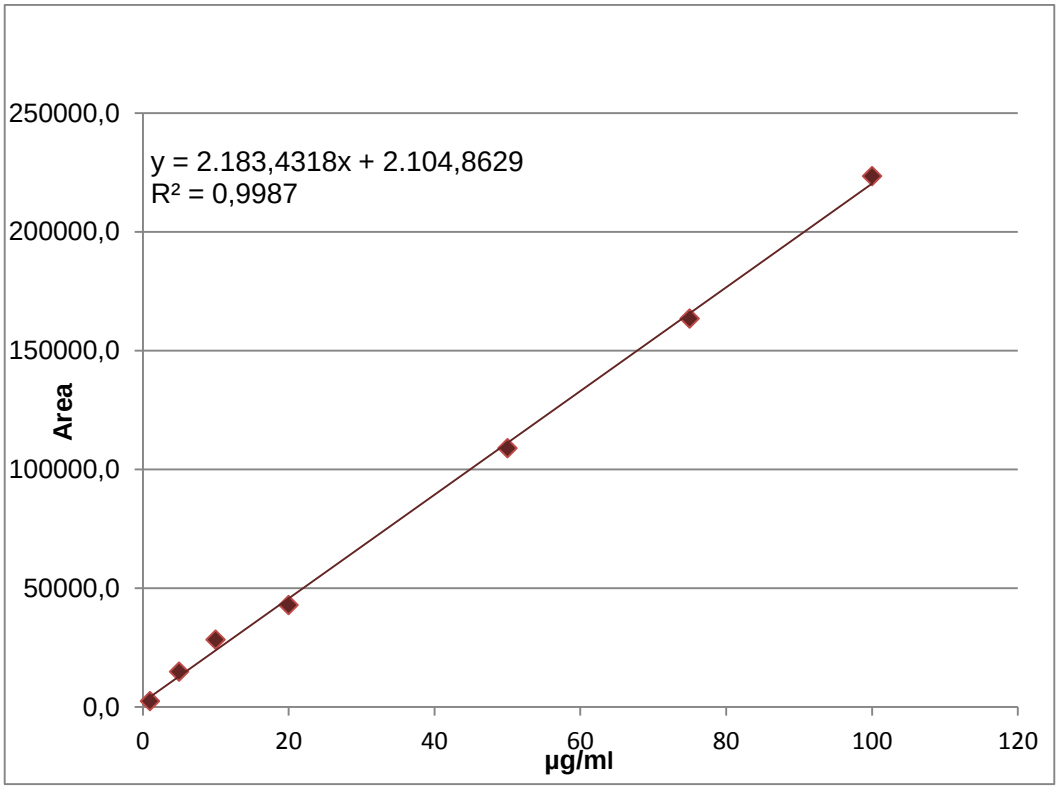

Figure 24 Calibration curve of FE@SUPPY:2

2.2.5. Autoradiography

A repellent barrier to maintain reagents localized on the tissue slices was created by drawing a circle around the tissue sections with the PAP pen. The section slides were preincubated and adjusted to room temperature with 50 mM cooled TRIS-HCl-Buffer (ph 7.41) and afterwards dried under the laminar air flow.

The solution for the experiment was prepared in an Eppendorf Tube and 40µl of it were applied per slice of tissue. The concentration of the antagonists and the agonist was calculated according to the following K_i/K_D:

DPCP:	k_i=0.46 µM
SCH 442416:	k_i=0.048 µM
MRS 1191:	k_i=31 nM
FE@SUPPY:	k_i=4.2 nM
FE@SUPPY:2:	k_i=4.2 nM
I-AB-MECA:	k_D=0.6 nM

Table 3 Chosen antagonists/agonist and according k_i/k_D

Experimental scheme

1. Baseline

[^{18}F]FE@SUPPY/[^{18}F]FE@SUPPY:2/[^{125}I]-AB-MECA + TRIS-HCl Buffer

2. Blocking of A_1, A_{2A}, A_{2B}

[^{18}F]FE@SUPPY/[^{18}F]FE@SUPPY:2/[^{125}I]-AB-MECA + DPCPX + SCH 442416 + MRS 1754 + TRIS-HCl Buffer

3. Blocking of A_1, A_{2A}, A_{2B}, A_3

[^{18}F]FE@SUPPY/[^{18}F]FE@SUPPY:2/[^{125}I]-AB-MECA + DPCPX + SCH 442416 + MRS 1754 + MRS 1191 + TRIS-HCl Buffer

4. Blocking of A_1, A_{2A}, A_{2B}, A_3

[^{18}F]FE@SUPPY/[^{18}F]FE@SUPPY:2/[^{125}I]-AB-MECA + DPCPX + SCH 442416 + MRS 1754 + FE@SUPPY + TRIS-HCl Buffer

5. Blocking of A_1, A_{2A}, A_{2B}, A_3

[^{18}F]FE@SUPPY/[^{18}F]FE@SUPPY:2/[^{125}I]-AB-MECA + DPCPX + SCH 442416 + MRS 1754 + FE@SUPPY:2 + TRIS-HCl Buffer

6. Blocking of A_1, A_{2A}, A_{2B}, A_3

[^{18}F]FE@SUPPY/[^{18}F]FE@SUPPY:2/[^{125}I]-AB-MECA + DPCPX + SCH 442416 + MRS 1754 + I-AB-MECA + TRIS-HCl Buffer

7. Blocking of A_3

[^{18}F]FE@SUPPY/[^{18}F]FE@SUPPY:2/[^{125}I]-AB-MECA + MRS 1191 + TRIS-HCl Buffer

8. Blocking of A_3

[^{18}F]FE@SUPPY/[^{18}F]FE@SUPPY:2/[^{125}I]-AB-MECA + FE@SUPPY + TRIS-HCl Buffer

9. Blocking of A_3

[^{18}F]FE@SUPPY/[^{18}F]FE@SUPPY:2/[^{125}I]-AB-MECA + FE@SUPPY:2 + TRIS-HCl Buffer

10. Blocking of A_3

[^{18}F]FE@SUPPY/[^{18}F]FE@SUPPY:2/[^{125}I]-AB-MECA + I-AB-MECA + TRIS-HCl Buffer

The solution with the chosen radioligand in the concentration according to the k_i was applied on the tissue slices. Selective blocking agents for A_1AR, $A_{2A}AR$ and $A_{2B}AR$ to prevent interaction were added. After the incubation time, the section slides were washed twice with TRIS-HCl-buffer and with cold water. Subsequently, the section slides were dried in the laminar air flow for ten minutes.

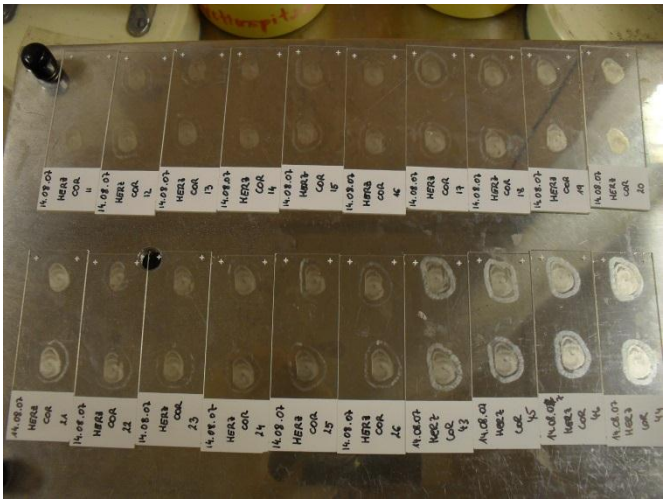

Figure 25 Slides with slices of brain sections [43]

The tissue slices were placed on the phosphor screen after drying. The exposure time differed based on the radioactivity of the radiotracer. For evaluating the results Optiquant© Image Analysis Software was used.

Figure 26 OptiQuant©Phosphor Imager [45]

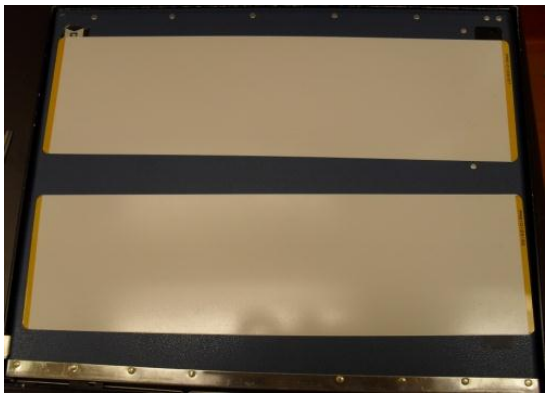

Figure 27 Phosphor screens [43]

In-vitro autoradiography was performed to quantify radioligand binding on a tissue by exposing it to phosphor screens. The radioactivity is detected by a thin layer of photostimulable BaFBr:Eu^{2+} phosphor crystals, protected by a moisture-proof coating. [46]

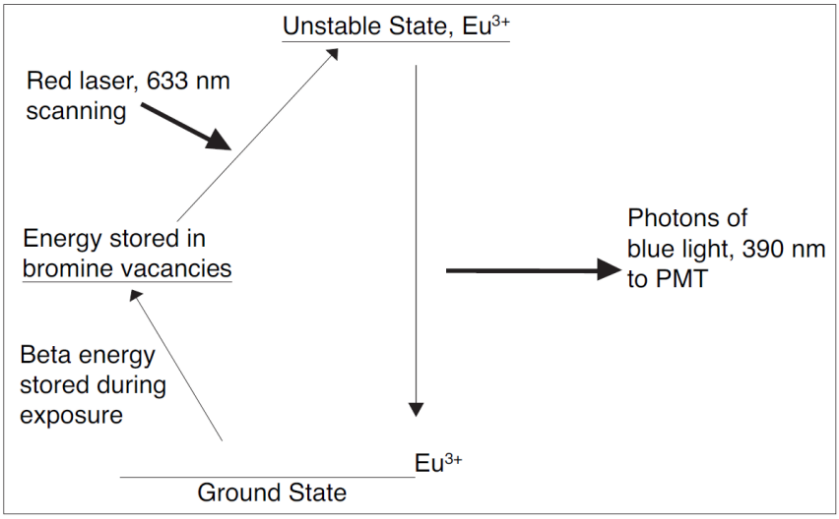

Figure 28 Schematic representation of the storage phosphor process [47]

The radioactive tissue samples were exposed to the phosphor screen, which absorbs and stores the energy. [46] By storing the emission, Eu^{2+} is oxidized to Eu^{3+} and the released electron is stored in the conduction band of the phosphor crystals, trapped in “F-Centers”. [47] At the end of the exposure time the phosphor imager uses a red laser (633 nm) to release the trapped electron and to convert Eu^{3+} to Eu^{2+}. Finally the stored energy is reemitted as blue light (390 nm), which is proportional to the radioactivity in the tissue sample. The photomultiplier tube detects the emission of the blue light and the data are stored as digital picture of locations and intensities. The screens can be used

for the next autoradiography after exposing them to white light from a light box and therefore erasing the stored images. [46]

2.2.6. Analysis with OptiQuant Image Analysis Software

The images were analysed with OptiQuant© Image Analysis Software. For the data and analysis of the rat brain sections, a chosen area of the hippocampus, the striatum, the cortex and additionally the whole brain slice was defined as region of interest. As a first step, template tags which can be changed in size and shape, were determined and placed on these regions. A rectangular tag was positioned on the hippocampus, ellipsoid tags on the striatum, cortex and the whole brain.

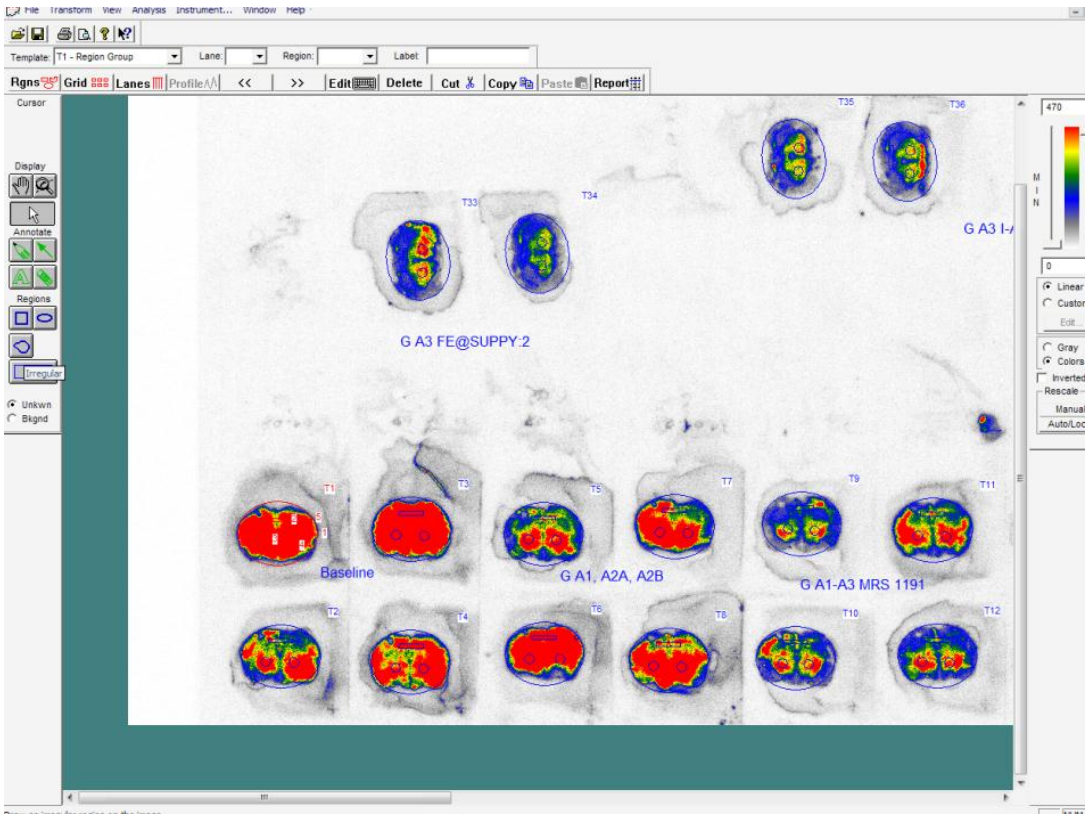

Figure 29 Optiquant© Phosphorimager Software [43]

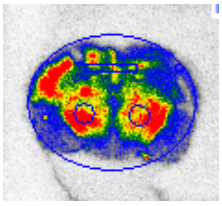

Figure 30 Analysis of rat brain sections with OptiQuant© Image Analysis Software [43]

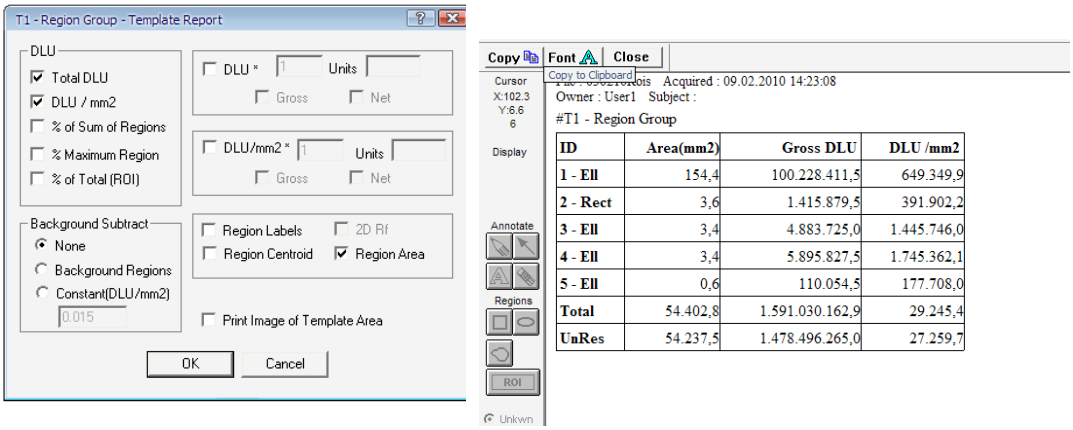

Figure 31 OptiQuant© Image Analysis Software [43]

The template tags were copied and placed on the remaining tissue samples. The application requests a format of the resulting report (Figure 31) before preparing data about the remaining activity on the samples. The decision was made to create a report, which presents the Digital Light Units (DLU) divided by the area of the cell in mm². The results were copied into an excel sheet and evaluation continued.

3. Results

3.1. [^{125}I]-AB-MECA

Experiments with rat brain slices, rat testes slices and rat heart slices were carried out. Interpretation of the results was implemented by relating measurements of regions of interest, which were set as 100% activity, to measurements of these regions when using different blocking agents.

3.1.1. Rat brain samples

Experiments with rat brain slices were performed with activity of 1.6 ± 0.15 kBq and exposure time of 89.63 ± 32.7 hours. The measurements of activity on the baseline sample were set as 100%.The regions of interest were as follows: Hippocampus, Striatum, Cortex and the brain section as a whole. The remaining activity was investigated when blocking A_1AR, A_{2A}R, A_{2B}AR and A_3AR and solely A_3AR with the blocking agents already described.

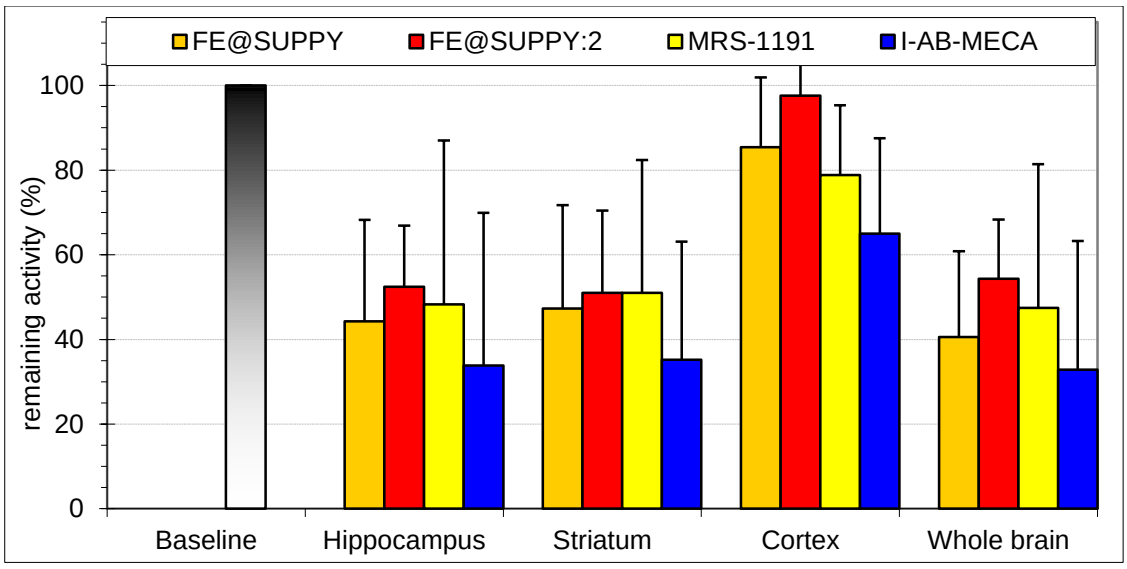

Figure 32 Remaining activity of [^{125}I]-AB-MECA when blocking A_1AR, A_{2A}AR, A_{2B}AR and A_3AR

Figure 32 shows less remaining activity on the whole brain when blocking with FE@SUPPY (40.56%) and applying unlabeled I-AB-MECA (32.82%) compared to blocking with FE@SUPPY:2 (54.34%) and MRS 1191 (47.42%). Furthermore, similar remaining activities were measured when blocking A_1AR-A_3AR with the chosen agents on the Hippocampus (FE@SUPPY:2: 52.46%; MRS 1191: 48.32%; FE@SUPPY: 44.27%) and on the Striatum (FE@SUPPY:2: 51.03%; MRS 1191: 50.98%;

FE@SUPPY: 47.34%). Use of unlabeled I-AB-MECA on the Hippocampus (33.84%) showed similar remaining activity like on the Striatum (35.21%). On the cortex highest remaining activity was examined when blocking A_3AR with FE@SUPPY:2 (97.58%). Blocking A_3AR on the cortex with FE@SUPPY (85.40%) resulted in higher remaining activity than use of MRS 1191 (78.87%). The use of unlabeled I-AB-MECA resulted in the highest remaining activity on the Cortex (64.97%) followed by similar activities on the Hippocampus (33.84%), Striatum (35.21%) and the whole brain (32.82%).

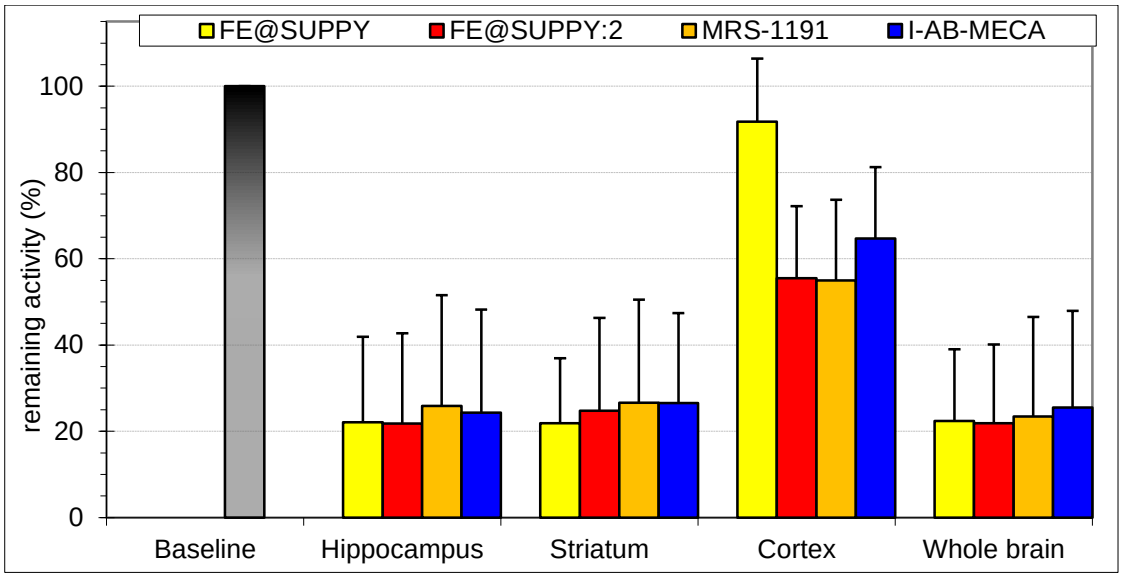

Figure 33 Remaining [^{125}I]-AB-MECA when only blocking A_3AR

Examining the remaining activity on the whole brain slice showed similar remaining activities when blocking with FE@SUPPY (22.40%), FE@SUPPY:2 (21.85%) and MRS 1191 (23.45%) and use of cold I-AB-MECA (25.50%). Almost the same results were observed on the Striatum when blocking with FE@SUPPY (21.86%), FE@SUPPY:2 (24.77%), MRS 1191 (26.63%) and using cold I-AB-MECA (26.54%). Results on the Cortex showed the highest remaining activity when blocking with FE@SUPPY (91.76%) and similar results when blocking with FE@SUPPY:2 (55.47%), MRS 1191 (55.01%) and using cold I-AB-MECA (64.66%).

3.1.2. Rat testes

Experiments with rat testes slices were performed with activity of 1.61 kBq and exposure time of 94.25 ± 1.06 hours.

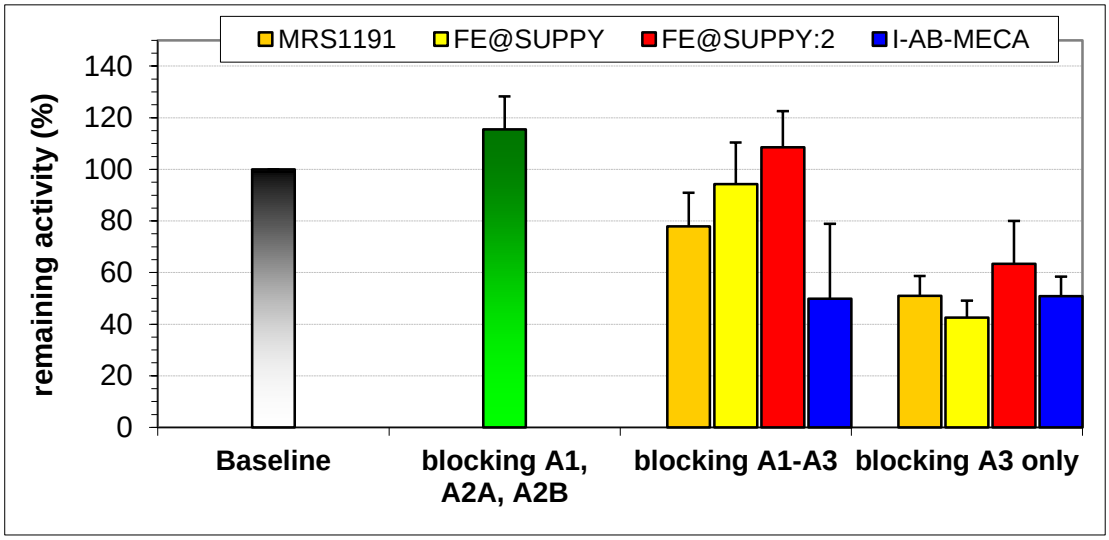

Figure 34 Experiments with [^{125}I]-AB-MECA using rat testis

Results showed high remaining activity (115.54%) when only blocking A_1AR, A_{2A}AR, A_{2B}AR. When blocking A_1AR, A_{2A}AR, A_{2B}AR and furthermore A_3AR, experiments revealed highest remaining activity when blocking with FE@SUPPY:2 (108.57%) and FE@SUPPY (94.23%) and less remaining activity when blocking with MRS 1191 (77.92%).

When blocking only A_3AR, results showed higher remaining activity when blocking with FE@SUPPY:2 (63.36%) and similar results when blocking with MRS 1191 (50.97%) and FE@SUPPY (42.58%). Use of unlabeled I-AB-MECA showed similar results when blocking A_1AR, A_{2A}AR, A_{2B}AR (49.91%) and only A_3AR (50.89%).

3.1.3. Rat heart

Experiments with rat heart slices were performed with activity of 1.54 ± 0.12 kBq and exposure time of 79.3 ± 26.27 hours.

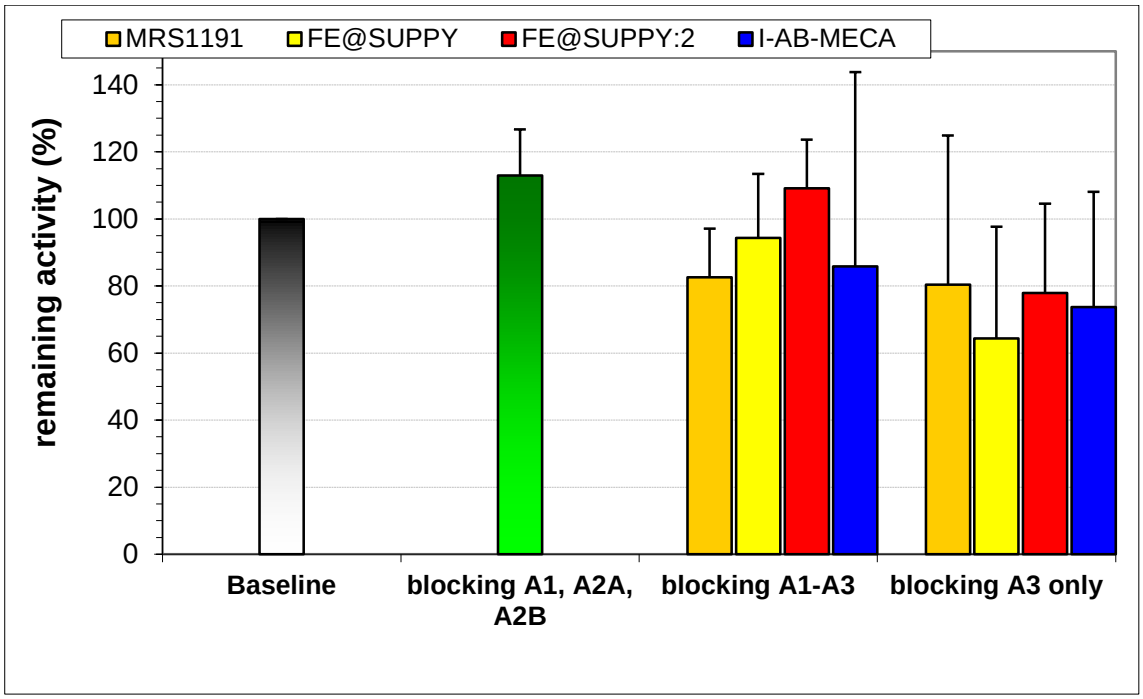

Figure 35 Experiments with [^{125}I]-AB-MECA using rat heart

Experiments on rat heart slices showed high remaining activity when only blocking A_1AR, A_{2A}AR, A_{2B}AR (112.99%). When blocking A_1AR, A_{2A}AR, A_{2B}AR and additionally A_3AR, the highest remaining activity was shown when blocking with FE@SUPPY:2 (109.13%), followed by FE@SUPPY (94.33%) and MRS1191 (82.6%). When blocking A_3AR results showed highest similar remaining activity when blocking with MRS 1191 (80.43%) and FE@SUPPY:2 (77.95%). FE@SUPPY showed less remaining activity (64.33%) than cold I-AB-MECA. Use of cold I-AB-MECA showed similar results when blocking A_1AR, A_{2A}AR, A_{2B}AR (85.78%) and only blocking A_3AR (73.67%).

3.2. [^{18}F]FE@SUPPY

Experiments with [^{18}F]FE@SUPPY on rat brain slices were performed with activity of 17.87 ± 9.25 kBq and exposure time of 14 ± 1.73 hours. The evaluation of the results was accomplished by comparing ratio of target/non-target when blocking with different agents.

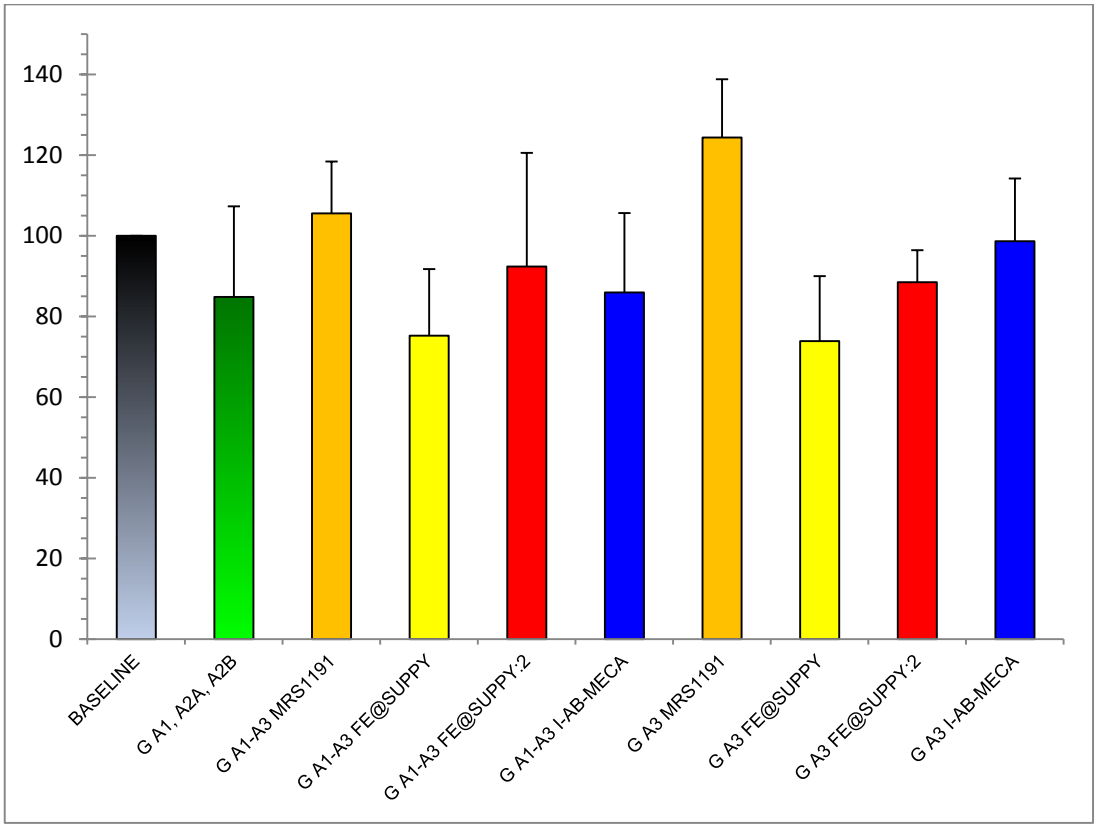

Figure 36 Ratio Hippocampus/Cortex of remaining activity of [^{18}F]FE@SUPPY

When blocking A_1AR, A_{2A}AR, A_{2B}AR, ratio Hippocampus/Cortex resulted in 84.84 % remaining activity. After blocking A_1AR, A_{2A}AR, A_{2B}AR and A_3AR, results showed higher ratio when blocking A_3AR with MRS 1191 (105.53 %) than with FE@SUPPY:2 (92.38%), FE@SUPPY (75.24%) and use of I-AB-MECA (85.96 %). When only blocking A_3AR with blocking agents, results showed higher ratio when performing the experiment with MRS1191 (124.31 %) than blocking with FE@SUPPY:2 (88.43 %), FE@SUPPY (73.90 %) and applying I-AB-MECA (98.65%).

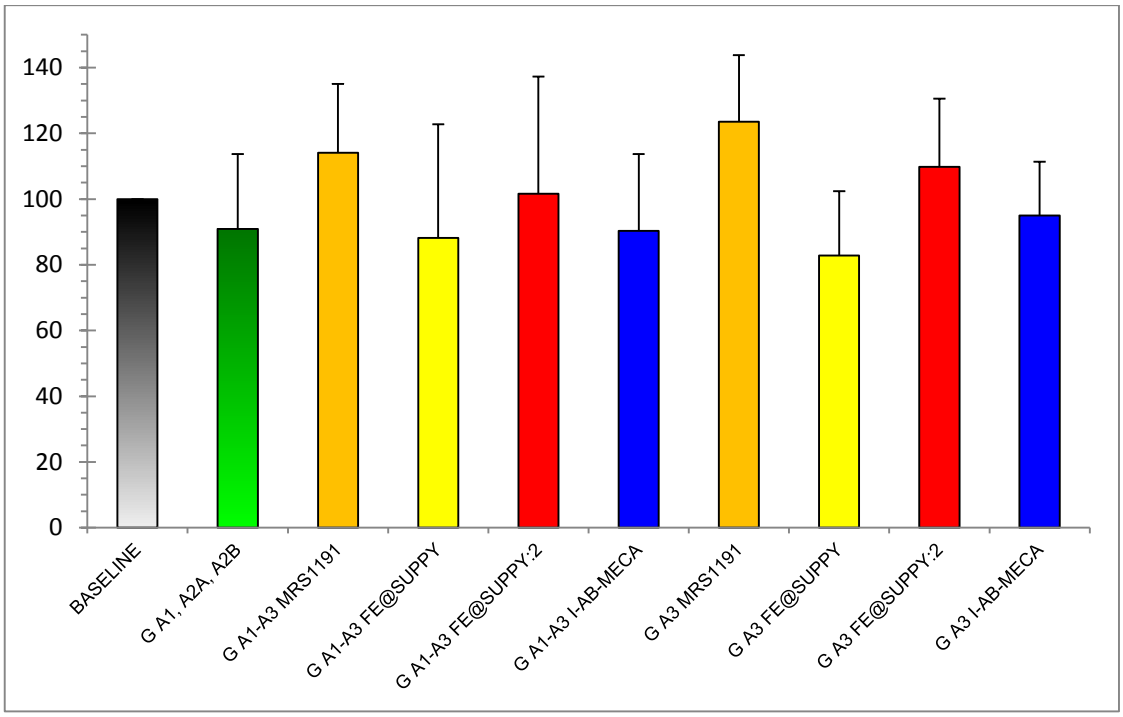

Figure 37 Ratio Striatum/Cortex of remaining activity of [^{18}F]FE@SUPPY

Evaluation of the experiments with [^{18}F]FE@SUPPY were furthermore implemented by comparing ratio of striatum/cortex when blocking with different agents. When blocking A_1AR, A_{2A}AR, A_{2B}AR ratio resulted in 90.88% remaining activity of [^{18}F]FE@SUPPY. When blocking A_1AR, A_{2A}AR, A_{2B}AR and A_3AR, results showed higher ratio when blocking with MRS 1191 (114.11%) than with FE@SUPPY:2 (101.63%), FE@SUPPY (88.22%) and use of I-AB-MECA (90.33%). When only blocking A_3AR results showed higher ratio when using MRS 1191 (123.54%), followed by FE@SUPPY:2 (109.79%), I-AB-MECA (94.99%) and FE@SUPPY (82.86%).

3.3. [^{18}F]FE@SUPPY:2

Experiments with [^{18}F]FE@SUPPY:2 on rat brain slices have been performed with activity of 26.19 ± 17.31 kBq and exposure time of 14.66 ± 1.03 hours.

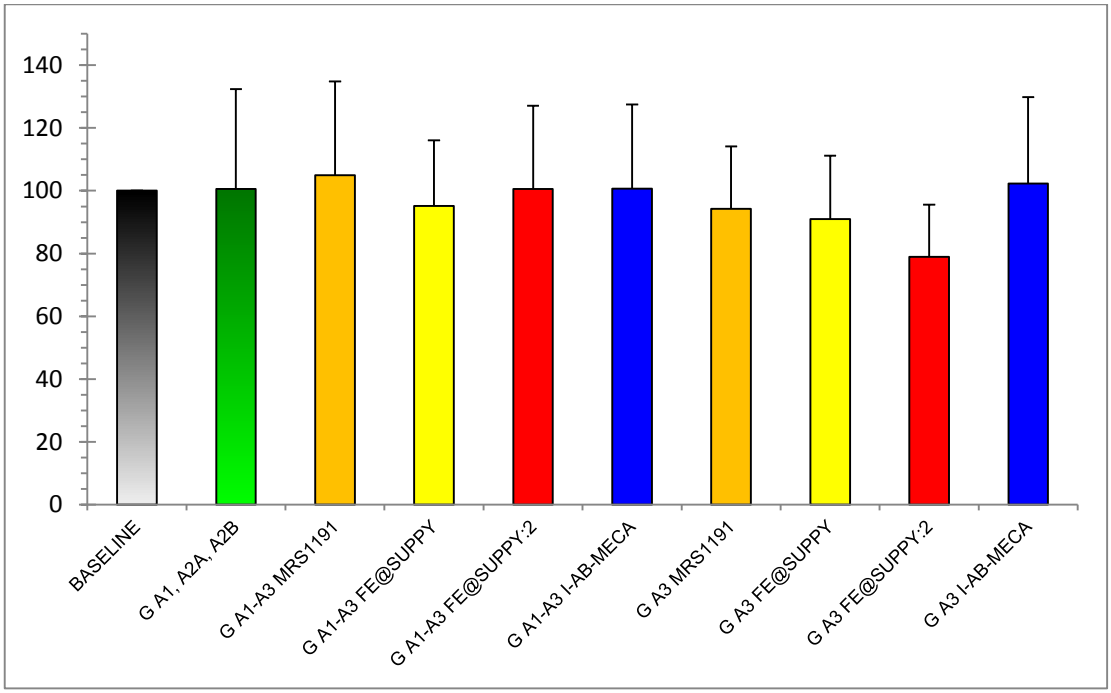

Figure 38 Ratio Hippocampus/Cortex of remaining activity of [^{18}F]FE@SUPPY:2

Calculation of ratio Hippocampus/Cortex resulted in 100.55% remaining activity of [^{18}F]FE@SUPPY:2, when blocking A_1AR, A_{2A}AR and A_{2B}AR. Similar ratios resulted when furthermore blocking A_3AR with MRS1191 (104.96%), FE@SUPPY (95.11%), FE@SUPPY:2 (100.52%) and I-AB-MECA (100.67%). After additionally blocking A_3AR I-AB-MECA (102.28%) showed highest ratio followed by MRS 1191 (94.25%), FE@SUPPY (90.99%) and FE@SUPPY:2 (78.91%).

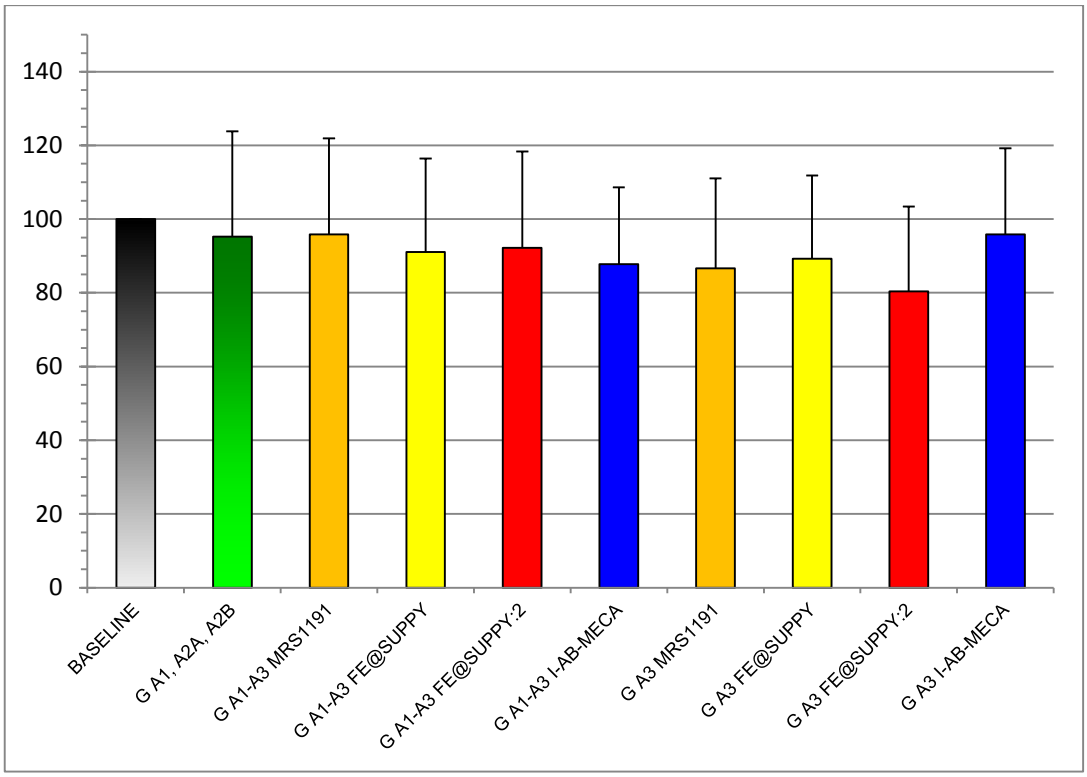

Figure 39 Ratio Striatum/Cortex of remaining activity of [^{18}F]FE@SUPPY:2

Calculation of ratio Hippocampus/Cortex resulted in 84.84% remaining activity of [^{18}F]FE@SUPPY:2, when blocking A_1AR, A_{2A}AR and A_{2B}AR. Furthermore, additional blocking of A_3AR was implemented with MRS1191 (105.53%), FE@SUPPY (95.11%), FE@SUPPY:2 (100.52%) and I-AB-MECA (100.67%). When only blocking A_3AR with blocking agents and an agonist, MRS1191 (124.31%) showed the highest ratio followed by I-AB-MECA (98.65%), FE@SUPPY (88.43%) and FE@SUPPY:2 (73.90%).

4. Discussion

The aim of this thesis was determined as the evaluation of specificity and affinity of [^{18}F]FE@SUPPY and [^{18}F]FE@SUPPY:2 by comparison with different blocking agents via autoradiography. Studies suggest a high affinity and selectivity of [^{18}F]FE@SUPPY for A_3AR and therefore expectations were high of the derivative FE@SUPPY:2, which binds ^{18}F at the thioester moiety instead of the carboxylic ester. Similar effects on the A_3AR were expected. Experiments to analyze the affinity of applied radiotracer and antagonists were performed by blocking A_1AR, A_{2A}AR and A_{2B}AR with selective blocking agents or only A_3AR.

Higher remaining activity was observed in studies on slices of rat heart, rat testes and rat brain by blocking A_1AR, A_{2A}AR, A_{2B}AR and A_3AR than by blocking only A_3AR. This increased binding of the radiotracer might be the result of interaction of the antagonists with the radiotracer.

Literature suggests high expression of A_3AR on the hippocampus and intermediate expression on striatum. [48]

Results proved this assumption and therefore the hippocampus und striatum were chosen as high target regions and cortex with less activity as non-target region.

Results of the experiments using [^{18}F]FE@SUPPY and [^{18}F]FE@SUPPY:2 as radiotracer, were disappointing. Due to the lipophilic structure, the compounds showed high nonspecific binding all over the brain section. Keeping the distribution of A_3R in mind, the evaluation was performed by calculating the ratio hippocampus/cortex and striatum/cortex.

[^{18}F]FE@SUPPY

Experiments with [^{18}F]FE@SUPPY showed the expected and desired labeling pattern in rat brain samples, despite its high nonspecific binding.

Blocking only A_1AR, A_{2A}AR, A_{2B}AR lead to a high ratio hippocampus/cortex and striatum/cortex, interpreted as interaction between the antagonists and the radiotracer.

The ratio hippocampus/cortex show lower affinity of MRS 1191 for A_3AR, both when blocking A_1AR, A_{2A}AR, A_{2B}AR or only A_3AR, compared to [^{18}F]FE@SUPPY as a consequence of the higher k_i values of 31 nM in contrast to k_i values of 4,2 nM. Similar results were shown by the ratio striatum/cortex.

Investigation of the ratio hippocampus/cortex and striatum/cortex of FE@SUPPY:2 revealed higher affinity for A_3AR than MRS 1191 when analyzing ratio hippocampus/cortex. This result was shown in experiments by additionally blocking A_1AR, A_{2A}AR, A_{2B}AR and by blocking only A_3AR. The affinity for A_3AR of FE@SUPPY:2 was expected to be equal or higher than MRS 1191 due to the related structure to FE@SUPPY and the findings proved this assumption.

Examination of the nonspecific binding of [^{18}F]FE@SUPPY was performed by evaluation of ratio hippocampus/cortex and striatum/cortex with applying FE@SUPPY or additional antagonists to block of A_1AR, A_{2A}AR, A_{2B}AR. The remaining activity of [^{18}F]FE@SUPPY could not be displaced by the unlabeled ligand and represents the nonspecific binding. Analysis showed high nonspecific binding of [^{18}F]FE@SUPPY conceivably due to the lipophilic structure.

Studies with FE@SUPPY:2 were expected to show similar ratios like FE@SUPPY because of the prior mentioned related structure to FE@SUPPY. Nonetheless, ratios of hippocampus/cortex and striatum/cortex of FE@SUPPY:2 showed lower affinity for A_3AR than FE@SUPPY irrespectively of only blocking A_3AR or additionally blocking A_1AR, A_{2A}AR and A_{2B}AR. This small change in the molecule probably affects non-covalent interactions e.g. halogen bonding between receptor and radiotracer and reduces affinity for A_3AR.

Examination of the ratio hippocampus/cortex revealed high affinity of I-AB-MECA for A_3AR, which is reflected by the k_D values of 0.6 nM. When additionally blocking A_1AR, A_{2A}AR, A_{2B}AR, higher affinity for A_3AR was shown by I-AB-MECA compared to FE@SUPPY:2 and MRS 1191. Investigation of the ratio hippocampus/cortex gained by experiments with I-AB-MECA without blocking A_1AR, A_{2A}AR, A_{2B}AR showed a higher amount of remaining [^{18}F]FE@SUPPY compared to the ratios of MRS 1191, FE@SUPPY and FE@SUPPY:2. Ratio of striatum/cortex revealed higher affinity of I-AB-MECA for the A_3AR compared to FE@SUPPY:2 and MRS 1191 and slightly lower affinity when comparing with FE@SUPPY. Analysis of the ratio striatum/cortex showed similar remaining activities of the high affinity ligand I-AB-MECA like blocking with FE@SUPPY. If taking the selectivity and affinity of I-AB-MECA into consideration, results of experiments with I-AB-MECA reflect probably the nonspecific binding of FE@SUPPY.

[^{18}F]FE@SUPPY:2

Experiments with [^{18}F]FE@SUPPY:2 demonstrate high remaining activity and high non-specific binding. Evaluation of results by calculation of the ratio hippocampus/cortex and

striatum/cortex revealed no unambiguous outcome due to the nonspecific binding. Despite the limited significance of the results, a trend is recognizable.

Analysis of the ratio hippocampus/cortex revealed higher remaining activity by blocking A_1AR, A_{2A}AR, A_{2B}AR compared to the baseline. The increased binding of [^{18}F]FE@SUPPY:2 can be explained, as previously stated, by a possible interaction between the antagonists and the radiotracer.

Results of the ratio hippocampus/cortex revealed MRS 1191 to show less affinity for A_3AR, both when blocking A_1AR, A_{2A}AR, A_{2B}AR or only the A_3AR, compared to FE@SUPPY as a consequence of the higher k_i values of 31 nM. Similar results with MRS 1191 were shown when the ratio striatum/cortex was interpreted. Identification of the potential to displace [^{18}F]FE@SUPPY:2 by using only antagonists for A_3AR, MRS 1191 showed better results than FE@SUPPY with regard to ratio striatum/cortex. Same results were shown when evaluating the ratio striatum/cortex.

Ratio striatum/cortex of experiments with FE@SUPPY and A_1AR, A_{2A}AR, A_{2B}AR antagonists displayed similar results like ratio hippocampus/cortex. FE@SUPPY exhibits higher affinity for A_3AR than MRS 1191, FE@SUPPY:2 and I-AB-MECA. By only blocking A_3AR with FE@SUPPY, the ratio hippocampus/cortex assumes slightly higher affinity of FE@SUPPY than MRS 1191 and I-AB-MECA. The ratio striatum/cortex suggests lower affinity of FE@SUPPY compared with MRS 1191 and slightly higher affinity than I-AB-MECA. Although these two regions of the rat brain were chosen as target regions, the evaluation yielded different results. Numerous factors might have led to this result e.g. lipophilicity which led to remaining antagonist in the pipette tips. Furthermore, density of receptors on this brain tissue is unknown, nonspecific binding of [^{18}F]FE@SUPPY:2 is apparent and so only limited assumptions about blocking qualities can be made.

Discussion of the ratio of hippocampus/cortex of [^{18}F]FE@SUPPY:2 with blocking additionally A_1AR, A_{2A}AR, A_{2B}AR, revealed slightly higher remaining activity compared to studies with I-AB-MECA. When only blocking A_3AR, FE@SUPPY:2 showed lowest remaining activity compared to MRS 1191, FE@SUPPY and I-AB-MECA. By investigating the ratio striatum/cortex, FE@SUPPY:2 displayed similar remaining activities as FE@SUPPY and I-AB-MECA, when blocking additionally A_1AR, A_{2A}AR, A_{2B}AR. Blocking only A_3AR showed lower remaining activity compared to MRS 1191, FE@SUPPY and I-AB-MECA. These results reflect the problem of lipophilicity of FE@SUPPY:2. The remaining activity of [^{18}F]FE@SUPPY:2 represents the non-specific binding, which can't be displaced by FE@SUPPY:2. Even if other antagonists or agonists

show higher affinity for A_3AR than FE@SUPPY:2, interpretation can only be performed with consideration of large amount of binding to other sites than A_3AR.

The ratio hippocampus/cortex and striatum/cortex of the high affinity ligand I-AB-MECA showed the same amount of remaining activity in experiments targeting only A_3AR or additionally blocking A_1AR, A_{2A}AR and A_{2B}AR. Due to the high nonspecific binding and the high remaining activity after application of this high affinity ligand, a reliable statement regarding the affinity of [^{18}F]FE@SUPPY:2 compared to I-AB-MECA is not possible.

[^{125}I]-AB-MECA

The data obtained from experiments with rat brain slices were analyzed by comparing the blocking potential of antagonists on certain regions of the brain section.

Blocking of A_1AR, A_{2A}AR, A_{2B}AR and additionally A_3AR with FE@SUPPY resulted in similar remaining activity on the hippocampus, striatum, cortex and the whole brain slice. The findings suggest a slightly better potential to block A_3AR than MRS 1191 and FE@SUPPY:2. Blocking A_1AR, A_{2A}AR, A_{2B}AR with antagonists and A_3AR with MRS 119 showed slightly higher remaining activity of [^{125}I]-AB-MECA compared to blocking with FE@SUPPY and slightly less remaining activity compared to blocking with FE@SUPPY:2 on the hippocampus. Evaluation of ratio striatum/cortex showed similar affinity for the A_3AR of MRS 1191 and FE@SUPPY:2. These antagonists seem to have slightly less affinity for A_3AR compared to FE@SUPPY. As previously discussed, MRS 1191 has higher k_i values than FE@SUPPY and thereby lower affinity for A_3AR, which is reflected in our findings. By analyzing the results of the cortex and the whole brain slice, findings demonstrate a higher affinity of MRS 1191 for A_3AR compared to FE@SUPPY. Experiments when applying I-AB-MECA while blocking A_1AR, A_{2A}AR, A_{2B}AR, showed similar and low remaining activity on hippocampus, striatum and the whole brain slice. The remaining activity represents binding to nonspecific sites, which can't be displaced by I-AB-MECA. In general, remaining activity on the cortex is higher than on the target regions due to the low density of A_3AR. Interestingly, the same blocking potential results on target regions are detected even on the non-target. Experiments performed by only blocking A_3AR with MRS 1191, FE@SUPPY and FE@SUPPY:2 showed low remaining activities despite the additional affinity of [^{125}I]-AB-MECA for A_1AR. MRS 1191, FE@SUPPY and FE@SUPPY:2 showed similar blocking potential on the target regions hippocampus and striatum as well as on the whole brain slice. Similar remaining activities resulted when applying I-AB-MECA. Experiments suggest high affinity of FE@SUPPY, FE@SUPPY:2 and MRS 1191 as the amount of the remaining activity correlates with the non-specific binding after performing experiments with I-AB-MECA.

By blocking A_1AR, A_{2A}AR, A_{2B}AR, experiments on rat testis sections showed high remaining activities as a possible result of interaction among the antagonists and [^{125}I]-AB-MECA. Blocking A_1AR, A_{2A}AR, A_{2B}AR and furthermore A_3AR, experiments revealed lowest potential to displace [^{125}I]-AB-MECA by FE@SUPPY. MRS 1191 showed greater ability to block A_3AR than FE@SUPPY. Blocking only A_3AR, FE@SUPPY:2 showed the lowest affinity for A_3AR and similar results were found by blocking with MRS 1191 and FE@SUPPY. Blocking A_1AR, A_{2A}AR, A_{2B}AR and applying additionally I-AB-MECA resulted in similar remaining activity of the antagonists. Results on rat testis slices showed comparable affinities of FE@SUPPY with MRS 1191 and lower affinity of FE@SUPPY:2.

Blocking A_1AR, A_{2A}AR, A_{2B}AR on rat heart slices and applying [^{125}I]-AB-MECA resulted in high remaining activity due to possible interaction among the antagonists and [^{125}I]-AB-MECA. Blocking A_1AR, A_{2A}AR, A_{2B}AR and additionally A_3AR, results showed lowest affinity for A_3AR again by FE@SUPPY:2. MRS1191 displays a slightly higher affinity for A_3AR than FE@SUPPY. Blocking A_3AR only resulted in highest affinity for A_3AR by FE@SUPPY. MRS 1191 and FE@SUPPY:2 showed similar abilities to displace [^{125}I]-AB-MECA. FE@SUPPY showed less remaining activity than unlabeled I-AB-MECA. I-AB-MECA showed similar results when additionally blocking A_1AR, A_{2A}AR, A_{2B}AR or only targeting A_3AR. Experiments with rat heart slices showed again similar potential of FE@SUPPY to block A_3AR. FE@SUPPY:2 represents again the antagonist with lowest affinity for A_3AR.

5. Conclusion

Experiments with [^{125}I]-AB-MECA showed better or equal blocking potential of FE@SUPPY compared to MRS 1191. FE@SUPPY:2 proved its affinity for A_3AR, although not to the extent that was expected. Due to the higher k_i values of MRS 1191, results of FE@SUPPY weren't surprising.

FE@SUPPY was expected to show similar affinity for A_3AR like FE@SUPPY. Results showed lower affinity than FE@SUPPY and MRS 1191. The lower affinity might be a consequence of the loss of a non-covalent bonding between radiotracer and receptor.

Experiments showed higher remaining activity when blocking A_1AR, A_{2A}AR, A_{2B}AR and A_3AR than by blocking only A_3AR. This increased binding of the radiotracer might be the result of interaction of the antagonists with the radiotracer. By comparing the results of experiments with blocking all subtypes/only A_3AR, findings revealed a higher radioactive

signal of the tracer but no significant difference of blocking potential of the A_3AR antagonists based on the interaction.

Both FE@SUPPY and FE@SUPPY:2 showed high nonspecific binding on rat brain, rat testis and rat brain slices as a result of the lipophilic structure. Interestingly, the amount of nonspecific binding does not differ significantly within and between experiments performed by blocking all receptor subtypes or only A_3AR. [^{125}I]-AB-MECA showed in experiments on rat brain sections nonspecific binding in a not negligible scale. Experiments on rat brain sections revealed nonspecific binding more than half as much as [^{18}F]FE@SUPPY and [^{18}F]FE@SUPPY:2.

Literature suggests a higher distribution of A_3ARs in rat testis than in rat heart and little distribution in rat brain. Experiments with [^{125}I]-AB-MECA showed the expected labelling pattern on rat brain with radioactive signals on hippocampus, striatum and cerebellum. Experiments with rat testis were successfully completed but results are not available in sufficient quantities due to a device malfunction. As described in literature, experiments on rat hearts showed low A3AR density and consequently high remaining activity.

6. Outlook

The four adenosine receptors have been suggested in several studies as therapeutic targets in various diseases. The A_3AR subtype is involved in many cytoprotective functions such as anti-inflammatory, anticancer and cardioprotective effects. [1] PET is a widely used imaging technique to detect or follow the progress of certain pathophysiological conditions or receive knowledge about receptors in the living organism.

[^{18}F]FE@SUPPY was developed as the first PET tracer targeting the A_3AR. Its derivative [^{18}F]FE@SUPPY:2 was presented as a possible successor of [^{18}F]FE@SUPPY. The results reflect the affinity of our radiotracer for A_3AR rat tissue. Studies suggest interspecies differences of A_3AR and so the outcome of our experiments cannot be transferred to human A_3AR. [10] The next step would be to implement studies on human tissue and evaluate affinity of [^{18}F]FE@SUPPY and [^{18}F]FE@SUPPY:2 for human A_3AR.

A satisfactory radiotracer shows high affinity, high selectivity and low unspecific binding for the target receptor. [38] Both [^{18}F]FE@SUPPY and [^{18}F]FE@SUPPY:2 showed high unspecific binding due to the lipophilic structure. Our results suggest future studies on derivatives with a less lipophilic structure.

7. Appendix

7.1. Raw data

7.1.1. Calibration Curve of FE@SUPPY

µg/ml	Area 1	Area 2	Area 3	Area 4	Area 5	Area 6	Average value	Standard deviation
1	2698	2470	2351,5	2108,0	2130	2123,0	2313,4167	239,15234
5	11130,0	10819	10891,0	11130,0	10819	10891,0	10946,667	145,6141
10	26177,0	24877,0	25911,0	16460,0	26838,0	22123,0	23731	3928,2359
20	49437,0	49024,0	48911,0	45565,0	49814,0	54659,0	49568,333	2923,9546
50	119865,0	124917,0	120416,0	125110,0	123647,0	122715,0	122778,33	2228,7794
75	180052,0	181707,0	185152,0	175381,0	177373,0	181981,5	180274,42	3497,7268
100	238265,0	247493,0	253647,0	242534,5	244820,0	236969	243954,75	6170,8776

Table 3 Calibration Curve of FE@SUPPY

7.1.2. Calibration Curve of FE@SUPPY:2

µg/ml	Area 1	Area 2	Area 3	Area 4	Area 5	Area 6	Average Value	Standard deviation
1	2352,0	2287,0	2081,0	2886	2580	2840	2504,3	292,6081946
5	14236,0	12645,0	12771,0	17116	16731	15987	14914,33333	1802,873416
10	29934,5	30052,0	33374,0	25321,0	25440,0	26100,0	28370,25	2981,917752
20	41556,0	39389,0	38556,0	46029,0	45988,0	46071,0	42931,5	3224,372432
50	103231,0	104775,0	106739,0	112804,0	113500,0	112770,5	108969,9167	4186,799956
75	163679,0	164953,0	165384,0	163020,0	162910,0	161003,5	163491,5833	1443,565794
100	238299,5	222452,0	229047,0	221220,0	210931,0	218617,5	223427,8333	8542,817961

Table 4 Calibration Curve of FE@SUPPY:2

7.1.3. [^{125}I]-AB-MECA - Rat brain samples

	Hippocampus	Striatum	Cortex	Whole Brain
MRS 1191	48,32083	50,97687	78,86509	47,42419
FE@SUPPY	44,26839	47,33625	85,39613	40,55843
FE@SUPPY:2	52,46096	51,02947	97,57569	54,33564
I-AB-MECA	33,83634	35,21491	64,9698	32,82281

Table 5 Average value of remaining activity in % of [^{125}I]-AB-MECA when blocking A_1AR, A_{2A}R, A_{2B}AR and A_3AR

	Hippocampus	Striatum	Cortex	Whole Brain
MRS 1191	38,72752	31,44342	16,48077	33,98092
FE@SUPPY	24,00385	24,37758	16,54234	20,30015
FE@SUPPY:2	14,44095	19,40935	37,64106	13,97968
I-AB-MECA	36,04882	27,86858	22,54016	30,45324

Table 6 Standard deviation of remaining activity in % of [^{125}I]-AB-MECA when blocking A_1AR, A_{2A}R, A_{2B}AR and A_3AR

	Hippocampus	Striatum	Cortex	Whole Brain
MRS 1191	25,84759	26,63487	55,00538	23,44934
FE@SUPPY	22,07727	21,86025	91,76623	22,3998
FE@SUPPY:2	21,79734	24,77367	55,47177	21,84884
I-AB-MECA	24,32354	26,53912	64,66422	25,50496

Table 7 Average value of remaining activity in % of [^{125}I]-AB-MECA when only blocking A_3AR

	Hippocampus	Striatum	Cortex	Whole Brain
MRS 1191	25,70374	26,63487	18,63363	23,03983
FE@SUPPY	19,83817	15,10962	14,63234	16,6166
FE@SUPPY:2	20,94644	21,50526	16,68712	18,31486
I-AB-MECA	23,88643	20,86783	16,54973	22,41972

Table 8 Standard deviation of remaining activity in % of [^{125}I]-AB-MECA when only blocking A_3AR

7.1.4. Remaining activity of [^{125}I]-AB-MECA - Rat testis samples

	Blocking A_1, A_{2A}, A_{2B}	Blocking A_1-A_3	Blocking A_3
	121,9837		
MRS 1191		75,46413	64,5262
FE@SUPPY		76,36642	38,18833
FE@SUPPY:2		76,36642	47,4968
I-AB-MECA		106,1822	57,08015

Table 9 Average value of remaining activity in % of [^{125}I]-AB-MECA in rat testis slices

	Blocking A_1, A_{2A}, A_{2B}	Blocking A_1-A_3	Blocking A_3
	24,87035		
MRS 1191		25,62634	20,70009
FE@SUPPY		16,55701	6,070513
FE@SUPPY:2		21,06276	18,81604
I-AB-MECA		65,60676	10,38453

Table 10 Standard deviation of remaining activity in % of [^{125}I]-AB-MECA in rat testis slices

7.1.5. Remaining activity of [^{125}I]-AB-MECA - Rat heart samples

	Blocking A_1, A_{2A}, A_{2B}	Blocking A_1-A_3	Blocking A_3
	112,9884		
MRS 1191		82,60171	80,43024
FE@SUPPY		94,3256	64,33047
FE@SUPPY:2		109,1326	77,95276
I-AB-MECA		85,7852	73,67176

Table 11 Average value of remaining activity in % of [^{125}I]-AB-MECA in rat heart slices

	Blocking A_1, A_{2A}, A_{2B}	Blocking A_1-A_3	Blocking A_3
	13,75248		
MRS 1191		14,48154	44,49607
FE@SUPPY		19,0838	33,32287
FE@SUPPY:2		14,53915	26,6102
I-AB-MECA		58,03936	34,39322

Table 12 Standard deviation of remaining activity in % of [^{125}I]-AB-MECA in rat heart slices

7.1.6. [^{18}F]FE@SUPPY - Rat brain samples

	Blocking A_1, A_{2A}, A_{2B}	Blocking A_1-A_3	Blocking A_3
	84,84		
MRS 1191		105,53	124,31
FE@SUPPY		75,24	73,90
FE@SUPPY:2		92,38	88,43
I-AB-MECA		85,96	98,65

Table 13 Ratio target/non-target – Hippocampus/Cortex

	Blocking A_1, A_{2A}, A_{2B}	Blocking A_1-A_3	Blocking A_3
	90,88		
MRS 1191		114,11	123,54
FE@SUPPY		88,22	82,86
FE@SUPPY:2		101,63	109,79
I-AB-MECA		90,33	94,99

Table 14 Ratio target/non-target – Striatum/Cortex

7.1.7. [^{18}F]FE@SUPPY:2 - Rat brain samples

	Blocking A_1, A_{2A}, A_{2B}	Blocking A_1-A_3	Blocking A_3
	100,55		
MRS 1191		104,96	94,25
FE@SUPPY		95,11	90,99
FE@SUPPY:2		100,52	78,91
I-AB-MECA		100,67	102,28

Table 15 Ratio target/non-target – Hippocampus/Cortex

	Blocking A_1, A_{2A}, A_{2B}	Blocking A_1-A_3	Blocking A_3
	95,22		
MRS 1191		95,80	86,66
FE@SUPPY		91,08	89,28
FE@SUPPY:2		92,20	80,37
I-AB-MECA		87,73	95,84

Table 16 Ratio target/non-target – Striatum/Cortex

7.2. Figures

7.3. Schemes

7.4. Tables

7.5. References

[1] Jacobson KA. Introduction to adenosine receptors as therapeutic targets. in: Wilson CN., Mustafa SJ., editors. Adenosine Receptors in Health and Disease. 2009 Vol.193. Springer Verlag, Berlin, Heidelberg *Handb Exp Pharmacol*:1-24.

[2] Jacobson KA., Gao ZG. Adenosine receptors as therapeutic targets. 2006 *Nat Rev Drug Discov*; 5:247-64.

[3] Hunnius, Pharmazeutisches Wörterbuch.1998 *Walter de Gruyter: Berlin, New York, 8th Edition*: 19.

[4] Sachdeva S., Gupta M. Adenosine and its receptors as therapeutic targets: An overview. 2013 *Saudi Pharm J*; 21:245-53.

[5] Baraldi PG., Cacciari B., Romagnoli R., Merighi S., Varani K., Borea PA., et al. A_3 Adenosine receptor ligands: history and perspectives. 2000 *Med Res Rev*; 20:103-28.

[6] van Calker D., Muller M., Hamprecht B. Adenosine regulates via two different types of receptors, the accumulation of cyclic cAMP in cultured brain cells. 1979 *J Neurochem*; 33:999-1005.

[7] Zezula J., Freissmuth M. The A_{2A}-adenosine receptor: a GPCR with unique features? 2008 *British Journal of Pharmacology*; 153:184-190.

[8] Poulsen, SA, Quinn RJ, Adenosine receptors: new opportunities for future drugs. 1998 *Bioorg Med Chem*; 6:619-41.

[9] Mustafa SJ., Morrison RR., Teng B., Pelleg A. Adenosine receptors and the heart: role in regulation of coronary blood flow and cardiac electrophysiology. in: Wilson CN., Mustafa SJ., editors. Adenosine Receptors in Health and Disease. 2009 Vol.193. Springer Verlag, Berlin, Heidelberg *Handb Exp Pharmacol*:161-88.

[10] Borea PA., Gessi S., Bar-Yehuda S., Fishman P. A_3 adenosine receptor: pharmacology and role in disease. in: Wilson CN., Mustafa SJ., editors. Adenosine Receptors in Health and Disease. 2009 Vol.193. Springer Verlag, Berlin, Heidelberg *Handb Exp Pharmacol*:297-327.

[11] Chen JF., Eltzschig HK., Fredholm BB. Adenosine receptors as drug targets—what are the challenges? 2013 *Nat Rev Drug Discov*; 12:265-86.

[12] Wendler CC., Amatya S., McClaskey C., Ghatpande S., Fredholm BB., Rivkees SA. A_1 adenosine receptors play an essential role in protecting the embryo against hypoxia. 2007 *Proc Natl Acad Sci U S A*; 104:9697-702.

[13] DPCPX: 24.02.2014 http://www.sigmaaldrich.com/catalog/product/sigma/c101?lang=de&region=AT

[14] Kiesman WF., Elzein E., Zablocki J. A_1 adenosine receptor antagonists, agonists, and allosteric enhancers. in: Wilson CN., Mustafa SJ., editors. Adenosine Receptors in

Health and Disease. 2009 Vol.193. Springer Verlag, Berlin, Heidelberg *Handb Exp Pharmacol*:25-58.

[15] Baraldi PG., Tabrizi MA., Gessi S., Borea PA. Adenosine receptor antagonists: translating medicinal chemistry and pharmacology into clinical utility. 2008 *Chem Rev;* 108:238-63.

[16] SCH 442416 24.02.2014 http://www.sigmaaldrich.com/catalog/product/sigma/s6451?lang=de&region=AT

[17] Polosa R., Blackburn MR., Adenosine receptors as targets for therapeutic intervention in asthma and chronic obstructive pulmonary disease. 2009*Trends Pharmacol Sci;* 30:528-35.

[18] MRS 1754: 24.02.2014 http://www.sigmaaldrich.com/catalog/product/sigma/m6316?lang=de&region=AT

[19] Kalla RV., Zablocki J., Tabrizi MA., Baraldi PG. Recent developments in A_{2B} adenosine receptor ligands. in: Wilson CN., Mustafa SJ., editors. Adenosine Receptors in Health and Disease. 2009 Vol.193. Springer Verlag, Berlin, Heidelberg *Handb Exp Pharmacol*:99-122.

[20] Jacobson KA, Klutz AM, Tosh DK, Ivanov AA, Preti D, Baraldi PG., Medicinal chemistry of the A_3 adenosine receptor: agonists, antagonists, and receptor engineering. in: Wilson CN., Mustafa SJ., editors. Adenosine Receptors in Health and Disease. 2009 Vol.193. Springer Verlag, Berlin, Heidelberg *Handb Exp Pharmacol*:123-59.

[21] Abbrachio MP., Cattabeni F. Brain adenosine receptors as targets for therapeutic intervention in neurodegenerative diseases. 1999 *Ann N Y Acad Sci*; 890:72-92.

[22] Fishman P., Bar-Yehuda S., Synowitz M., Powell JD., Klotz KN., Gessi S., Adenosine receptors and cancer. in: Wilson CN., Mustafa SJ., editors. Adenosine Receptors in Health and Disease. 2009 Vol.193. Springer Verlag, Berlin, Heidelberg *Handb Exp Pharmacol*: 399-441.

[23] MRS 1191 24.02.2014 http://www.sigmaaldrich.com/catalog/product/sigma/m227?lang=de&region=AT

[24] Mitterhauser M, Haeusler D, Mien LK, Ungersboeck J, Nics L, Lanzenberger RR Automatisation and First Evaluation of [^{18}F]FE@SUPPY:2, an alternative PET-Tracer for the Adenosine A_3 Receptor: A comparison with [^{18}F]FE@SUPPY. 2009 *Open Nucl Med J*: 15-23.

[25] Li AH, Moro S, Forsyth N, Melman N, Ji XD, Jacobson KA. Synthesis, CoMFA analysis, and receptor docking of 3,5-diacyl-2,4-dialkylpyridine derivatives as selective A_3 adenosine receptor antagonists. 1999 *J Med Chem* 42:706-21.

[26] Wadsak W., Mien LK., Shanab K., Ettlinger DE., Haeusler D., Sindelar K., Preparation and first evaluation of [^{18}F]FE@SUPPY: a new PET tracer for the adenosine A_3 receptor. 2008 *Nucl Med Biol*; 35:61-6.

[27] Shearman LP, Weaver DR, [^{125}I]4-aminobenzyl-5'-N-methylcarboxamidoadenosine (^{125}I-AB-MECA) labels multiple adenosine receptor subtypes in rat brain. 1997 *Brain Res*; 745:10-20.

[28] [^{125}I]-AB-MECA 24.02.2014 http://www.perkinelmer.com/Catalog/Product/ID/NEX312010UC

[29] Forth H, Rummel, Förstermann, Starke, Allgemeine und spezielle Pharmakologie und Toxikologie. 2001 8th edition, *Urban & Fischer,* München, Jena

[30] Hulme EC., Trevethick MA. *Ligand binding assays at equilibrium: validation and interpretation*. 2010 *Br J Pharmacol*; 161:1219-37.

[31] L'Annunziata MF. Radioactivity: Introduction and History. 2007 *Elsevier,* Amsterdam

[32] Saha GB. Fundamentals of Nuclear Pharmacy 2010 6th edition, *Springer Verlag*, New York, Heidelberg, Dordrecht, London

[33] Khali, M., *Basic Sciences of Nuclear Medicine*. 2011 *Springer Verlag*, Berlin Heidelberg

[34] Levin C. Basic Physics of Radionuclide Imaging. in: Wernick MN., Aarsvold JN., Emission tomography- the fundamentals of PET and SPECT 2004 Amsterdam, Boston: *Elsevier Academic Press*: 53-88.

[35] Smith BT. Nuclear Pharmacy concepts and applications. 2010 *Pharmaceutical Press,* London

[36] ^{99}Mo/^{99m}Tc generator 24.02.2014 http://nucleus.iaea.org/HHW/Radiopharmacy/VirRad/Eluting_the_Generator/Generator_Module/Design_principles/index.html

[37] Links JM. Nuclear Medicine Physics, Instrumentation, and Data Processing in Pharmaceutical Research. in: Burns HD., Gibson RE, Dannals RF, Siegl PKS., editors. Nuclear imaging in drug discovery, development, and approval. 1993, *Basel: Birkhäuser*: 11-31.

[38] Haeusler D., Nics L., Mien LK., Ungersböck J., Lanzenberger RR., Shanab K [^{18}F]FE@SUPPY and [^{18}F]FE@SUPPY:2-metabolic considerations. 2010 *Nucl Med Biol*; 37:421-6

[39] Wernick MN., Aarsvold JN. Introduction to emission tomography. in: Emission tomography- the fundamentals of PET and SPECT. 2004 Amsterdam, Boston; *Elsevier Academic Press*: 11-23.

[40] Standard process for generating PET imaging 24.02.2014 http://www.sepscience.com/Sectors/Pharma/Articles/429-/Radio-IC-for-Quality-Control-in-PET-Diagnostics

[41] Iversen LL. Nuclear Imaging in Drug Development-Introduction. in: Burns HD., Gibson RE, Dannals RF, Siegl PKS., editors. Nuclear imaging in drug discovery, development, and approval. 1993, *Basel: Birkhäuser*: 1-9.

[42] Baker, JR. *Autoradiography: a comprehensive overview*. 1989, Oxford: *Oxford University Press*

[43] Own illustration

[44] Dissection of rat: 24.02.2014
http://jrsowash.wikispaces.com/file/view/rat.student.pdf

[45] Cyclone Plus Phosphor Imager from Perkin Elmer
http://www.biocompare.com/22067-Radioisotope-Imaging-Phosphor-Imaging-Phosphorimager/1899794-Cyclone-Plus-Phosphor-Imager/?ncatid=22067&ppim=1899794_4_0

[46] Johnström P., Bird JL., Davenport AP. Quantitative phosphor imaging autoradiography of radioligands for positron emission tomography. 2012 *Methods Mol Biol*; 897:205-20.

[47] Cyclone Plus Storage Phosphor Screen Performance and Application Guide 24.02.2014
http://www.perkinelmer.com/CMSResources/Images/44-73041APP_CyclonePlusStoragePhosphorScreen.pdf

[48] Lopes LV., Rebola N., Pinheiro PC., Richardson PJ., Oliveira CR., Cunha RA. Adenosine A3 receptors are located in neurons of the rat hippocampus. 2003 *Neuroreport*;14:1645-8.

Curriculum Vitae

ELISABETH SZERENCSICS

Geburtsdatum	28.9.1983
Geburtsort	Güssing, Burgenland Österreich

1990-1994 Volksschule Tobaj

1994-1998 Unterstufenrealgymnasium Oberschützen: *bilingualer Unterricht (Englisch/Deutsch)*

1998-2002 Oberstufenrealgymnasium Oberschützen

2002-2003 Studium der Technischen Physik an der TU Wien

WS 2003- WS 2013 Studium der Pharmazie an der Universität Wien